A virtual inspection framework for precision manufacturing of aerofoil components

Makem, J. E., Ou, H., & Armstrong, C. G. (2012). A virtual inspection framework for precision manufacturing of aerofoil components. *Computer-Aided Design*, *44*(9), 858–874. https://doi.org/10.1016/j.cad.2012.04.002

Published in:
Computer-Aided Design

Document Version:
Early version, also known as pre-print

Queen's University Belfast - Research Portal:
Link to publication record in Queen's University Belfast Research Portal

General rights
Copyright for the publications made accessible via the Queen's University Belfast Research Portal is retained by the author(s) and / or other copyright owners and it is a condition of accessing these publications that users recognise and abide by the legal requirements associated with these rights.

Take down policy
The Research Portal is Queen's institutional repository that provides access to Queen's research output. Every effort has been made to ensure that content in the Research Portal does not infringe any person's rights, or applicable UK laws. If you discover content in the Research Portal that you believe breaches copyright or violates any law, please contact openaccess@qub.ac.uk.

Download date:05. May. 2023

Accepted Manuscript

A virtual inspection framework for precision manufacturing of aerofoil components

Jonathan E. Makem, Hengan Ou, Cecil G. Armstrong

PII: S0010-4485(12)00075-9
DOI: 10.1016/j.cad.2012.04.002
Reference: JCAD 1927

To appear in: *Computer-Aided Design*

Received date: 17 August 2011
Accepted date: 7 April 2012

Please cite this article as: Makem JE, Ou H, Armstrong CG. A virtual inspection framework for precision manufacturing of aerofoil components. *Computer-Aided Design* (2012), doi:10.1016/j.cad.2012.04.002

This is a PDF file of an unedited manuscript that has been accepted for publication. As a service to our customers we are providing this early version of the manuscript. The manuscript will undergo copyediting, typesetting, and review of the resulting proof before it is published in its final form. Please note that during the production process errors may be discovered which could affect the content, and all legal disclaimers that apply to the journal pertain.

ACCEPTED MANUSCRIPT

*Manuscript
Click here to view linked References

A Virtual Inspection Framework for Precision Manufacturing of Aerofoil Components

Jonathan E. Makem[1)], Hengan Ou[2)*] and Cecil G. Armstrong[1)]

[1)] School of Mechanical and Aerospace Engineering, Queen's University Belfast, Belfast, UK, BT9 5AH

[2)] Department of Mechanical, Materials and Manufacturing Engineering, University of Nottingham, Nottingham, UK, NG7 2RD

ABSTRACT

The finite element method plays an extremely important role in forging process design as it provides a valid means to quantify forging errors and thereby govern die shape modification to improve the dimensional accuracy of the component. However, this dependency on process simulation could raise significant problems and present a major drawback if the finite element simulation results were inaccurate. This paper presents a novel approach to assess the dimensional accuracy and shape quality of aeroengine blades formed from finite element hot-forging simulation. The proposed virtual inspection system uses conventional algorithms adopted by modern coordinate measurement processes as well as the latest free-form surface evaluation techniques to provide a robust framework for virtual forging error assessment. Established techniques for the physical registration of real components have been adapted to localise virtual models in relation to a nominal design model. Blades are then automatically analysed using a series of intelligent routines to generate measurement data and compute dimensional errors. The results of a comparison study indicate that the virtual inspection results and actual coordinate measurement data are highly comparable and the procedures registration and virtual inspection are computationally efficient, validating the approach as an effective and accurate means to quantify forging error in a virtual environment. Consequently, this provides adequate justification for the implementation of the virtual inspection system in the virtual process design, modelling and validation of forged aeroengine blades in industry.

Keywords: Virtual Inspection, Finite Element Modelling, Coordinate Measurement, Hot-Forging, Aeroengine Blades.

* Corresponding author.

Email addresses: j.makem@qub.ac.uk (Jonathan E. Makem), h.ou@nottingham.ac.uk (Hengan Ou), c.armstrong@qub.ac.uk (Cecil G. Armstrong).

ACCEPTED MANUSCRIPT

1. Introduction

As a result of the increasing demands to maximise the performance and quality of manufactured components within the aerospace industry, parts are inspected to ensure their features adhere to the geometrical and dimensional specifications. In particular, the inspection of complex parts comprising free-form geometry, such as forged aeroengine compressor blades, is becoming ever-more important due to requirements for higher precision and efficiency. The premise behind most inspection processes involves determining the extent to which a component deviates from a given set of specifications by comparing its actual shape to a nominal model. For quality assurance purposes, high precision dimensional measurement techniques are employed to evaluate the dimensional tolerance of forged aerofoil blades. Generally, these inspection processes may be categorised into two main groups, utilising either contact or non-contact measurement. The later acquires surface information without physically contacting the part using sensing devices such as laser/optical scanners, X-rays and CT scans [1]. The main limitation with this approach is that the measurement data may be affected by factors such as part colour, surface roughness, viewpoint and lighting [2]. Conversely, the contact inspection process of coordinate measurement is an effective measurement technique, providing both high accuracy and repeatability. The process employs a computer controlled coordinate measurement machine (CMM) to inspect the part automatically by moving a tactile probe along the workpiece surface, to measure the coordinates of individual contact points. In terms of forged blade inspection, CMM is by far the most commonly used tool owing to its ease of use, automation and measurement precision.

Compressor blades for aeroengine applications are normally manufactured using the closed die hot-forging process. Forging of the work material at elevated temperatures creates distortion due to thermal contraction and spring-back, and shape errors due to the elastic deflection of the die and forging press. In industry, due to the complexity of the hot-forging process, forging process design is often dependent upon forging trials requiring prolonged lead times and increased costs. This iterative process involves modifying the die shape by a fraction of the measured forging error until the blade dimensions are within the specified tolerance and the aerofoil errors are sufficiently reduced. Therefore, dimensional inspection forms an integral part of this process by providing the necessary feedback to control the entire design and manufacturing process and achieve the desired results.

In blade forging design and manufacturing, finite element analysis has been widely used to simulate the material flow, stress/strain-rate distribution, thermal behaviour and forming load/energy requirements in blade forging [3, 4]. By removing the need to conduct expensive forging trials, finite element simulation may also be used as a design tool to quantify forging errors and thereby govern die shape modification for improved dimensional accuracy [5]. However, in order to assess the accuracy

ACCEPTED MANUSCRIPT

of the forging errors on blade models generated from a forging simulation, it is necessary to verify the dimensional and shape accuracies via comparison to actual measurement data. Little research has been reported in this area.

The aim of this research is to develop a generic virtual inspection system to assess the dimensional accuracy of forged aerofoil blades in a virtual environment thereby allowing a fast, automated correlation between virtual forging design and actual forging production. Similar to the conventional procedure for measuring a physical blade, the inspection process for the virtual blade model comprises three main stages: part localisation, aerofoil section inspection and parameter analysis. Both the classical 3-2-1 approach [2] and the iterative closest point (ICP) method [1] are implemented in part localisation. Aerofoil profile tolerances, aerofoil thickness and angular deviations from the nominal shape at three sections along the blade are evaluated by the aerofoil section inspection and parameter analysis modules. As a means of validation, a case study is presented to compare actual measurement data with the virtual inspection results. The results indicate that although the 3-2-1 approach is computationally efficient, the ICP method provides a much better solution to the part localisation of the blade model. A statistical analysis revealed a strong correlation between the virtual inspection results and the coordinate measurement data.

The remainder of this paper is organised as follows: Section 2 provides a comprehensive review of recent research in the area of dimensional inspection with specific emphasis on aeroengine blades. Section 3 describes the main aspects of the virtual inspection system. A more detailed description of the relevant theories and methodologies for part localisation and blade inspection is reported in section 4. An overview of the inspection systems software framework is provided in Section 5. The results of a case study detailing a comparison between virtual inspection data and actual measurement data are presented and discussed in Section 6. Concluding remarks are reported in section 7.

2. Literature Review

A critique of the latest work and technological developments in the area of aeroengine blade inspection is provided in this section. Relevant topics such as localisation part registration, methods and procedures for measurement data acquisition, as well as tolerance evaluation algorithms and techniques for quantifying geometrical and dimensional discrepancies are discussed in detail.

2.1 Part Localisation Techniques

The process of part localisation, also known as registration, mathematically locates the part prior to inspection by determining a rigid body 3D coordinate transformation between the design coordinate system (DCS) and the measurement coordinate system (MCS). Traditionally, the design coordinate

ACCEPTED MANUSCRIPT

system is located using the six point principle or 3-2-1 approach [1, 2, 6]. For parts with regular features such as planar surfaces or cylindrical features, coordinate systems may be easily established. However, as aerofoil blades are largely composed of freeform surfaces, it is difficult to locate enough planar surfaces to act as datum planes [7]. Consequently, various localisation techniques have been developed for free-form surface inspection.

Based on a concept of finding the closest point set between two free-from surfaces, the iterative closest point (ICP) approach may be used to establish a 3D transformation matrix by aligning the two surfaces through an iterative process [8]. Huang *et al* described an ICP approach which minimises the sum of the squared distances between the measured points and their closest points (corresponding points) on the nominal surface, also known *a priori* [9]. A transformation matrix generated by the approach comprises six parameters which define the position and orientation of the coordinate frame. Using the pseudo-inverse method, the sum of the squared distances may be minimised iteratively between the respective point sets. Menq *et al* [10] proposed an optimal match algorithm to determine a rigid body transformation of one surface related to another, also based on least-squares minimisation. Ainsworth *et al* [11, 12] presented a localisation approach which required an initial manual input to gain an approximate alignment of the part. Subsequently, an ICP algorithm was applied for more accurate registration. Lai *et al* [13] proposed an algorithm for the registration of irregular shapes using the coordinate measurement process. The part localisation process comprised of a rough and fine alignment procedure to match the part coordinate of the CMM with the model coordinate of the CAD model.

The main drawback of the aforementioned localisation techniques when applied to the registration of aerofoil blades is that they provide only an approximate solution to a set of measured data. The solution varies when the number or location of points varies and therefore does not guarantee that the design coordinate system can be regenerated for inspection [14]. Also, the ICP approach only ensures registration when the measurement surface and nominal model are close enough in both 3D orientation and position, necessitating initial manual alignment in some cases [1]. Conversely, the process of free-form surface localisation with reference to design datums locates the measured surface data with respect to the design model using known datum references instead of the free-form surface itself. The main advantage of this approach is that it does not require the specification of the closest points on a model, thereby providing a simpler yet more robust registration procedure which can be easily implemented [12, 14].

Datum reference frames may also be defined by using elementary datum reference features such as planes and cylinders [14]. Coordinate systems may be established using the normal of a planar datum or the axis of a cylindrical surface. In terms of the measured part, datums are constructed by fitting the

ACCEPTED MANUSCRIPT

measurement points of a feature according to a least squares principle [1]. Li *et al* described an approach for localisation of sculptured surfaces with datums using the concept of Datum Direction Frame (DDF) [7]. The localisation process proposed by Hsu *et al* for aerofoil blade inspection used an iterative algorithm incorporating CMM measurement and a coordinate upgrading procedure [6, 14]. However, the process is prone to error if local deformations are present [15]. For example, if an aberration in the surface occurs at a datum point, the coordinate system will be incorrectly aligned.

2.2 Blade Measurement and Evaluation

In general, the conventional methodology for part validation of turbine blades using the coordinate measurement process involves evaluating the dimensional accuracy of the component along several aerofoil cross sections. Hsu *et al* [2] described a blade section inspection approach where three cross sectional profiles were measured at the base, mid and tip sections perpendicular to the stacking axis. The CMM employed a contour measurement mode, whereby each blade profile was measured at a constant height (z coordinate). Cardew-Hall *et al* [15] proposed a similar process for section inspection, whereby planes perpendicular to the stacking axis cut the aerofoil to generate spline profiles. The precision inspection system developed by Pahk *et al* obtained scanning path measurement coordinates by using coordinate data from the CAD nominal model [16].

Once the blade has been successfully localised, dimensional errors will still exist as a result of curvature change, blade thickness and twist [2]. As the section curvature and twist becomes greater along the length of the aerofoil, the discrepancy between the measurement data and the nominal sectional data becomes more exaggerated. Consequently, additional alignment procedures are required to compensate for this residual misalignment error [16]. By minimising the residual misalignment, the sectional measurement data may then be transformed and a new set of corresponding points are generated on the nominal section. The iterative process of transforming the measurement data and calculating the curve corresponding points continues until the convergence of computation.

The geometric design parameters of an aerofoil blade may be categorised into three groups: blade orientation and displacement, blade dimensions and profile tolerance [2]. The blade dimensions that are commonly inspected for comparative analysis include the chord length, the length of the leading/trailing edge to the stacking axis and the aerofoil thickness at the leading edge, centre and trailing edge, respectively. Blade orientation and displacement indicate the deviation of the position and orientation of the overall blade. Blade orientation is defined in terms of the orientation angle. Blade displacement relates to the deviation between the actual and basic stacking points, where the stacking points are the construction points about which each section is defined.

ACCEPTED MANUSCRIPT

Generally, the profile tolerance is used to identify the form error of an individual region on the blade section, including the pressure and suction surfaces. A tolerance zone is usually defined as the space between the offset boundaries of the nominal profile and thereby sets a limit for the variation of the form error. Often, the profile tolerance is quoted as a single value for each section and may be defined as the sum of the maximum errors on both sides of the nominal curve. Pahk *et al* [16] proposed a rigorous approach for profile tolerance evaluation based on the Tschebyscheff norm between the measurement data and the corresponding closest points data.

Statistical based methods may be used as a means of tolerance verification, whereby the standard deviation of the manufactured surface reflects how far the measured surface deviates from the nominal model. According to Huang *et al* [17], the deviation of a manufactured surface may be separated into deterministic error, d and random error, ε components. As the deterministic error is virtually removed after localisation, the deviation of the surface is dominated by the random component, which obeys a normal distribution. As the actual deviation value is unknown, it can be estimated from the sample data. Several example cases to test the approach were presented by both Huang *et al* [17] and Li *et al* [7]. In each case, after initial localisation of the part to the DCS using the DDF's, either the maximum deviation of the free-form surface was out of tolerance or the standard deviation was above the acceptable limit. However, after performing further localisation using an optimal match algorithm, based on an ICP approach, the aforementioned values were successfully reduced to within the required tolerance range.

3. Virtual Inspection System

This section provides an overview of the virtual inspection system. The first stage of virtual inspection involves registering or localising the part in relation to a nominal model. The system provides a conventional registration procedure using non-marginal datum points and datum features to localise the part and an alternative localisation algorithm for registering free-form surfaces based on least squares minimisation. After localisation, measurement data is generated and various blade dimensions and geometrical parameters are evaluated in the second and third phases of the process.

3.1 Model Localisation

The two forms of localisation offered by the system are the 3-2-1 approach and ICP localisation. The traditional 3-2-1 approach may be employed to establish the blades coordinate system, as shown in Figure 1. However, not all of the datum points are defined by basic datum features. In particular, the primary datum plane is determined by three points on the free-form concave surface of the blade, including P_1 and P_2 on the root section and P_3 on the tip section. The secondary datum plane is

constructed using the central axis of cylindrical features at each end of the blade, defined by P_4 and P_5. Finally, the tertiary datum plane, orthogonal to both previous datum planes is determined using the last datum point, P_6, located on the root block. The normal vectors of the aforementioned datum planes, shown in Figure 2, are defined by Eq. 1 - Eq. 3.

$$P = (P_3 - P_2) \times (P_3 - P_1) \quad \text{Eq. 1}$$

$$S = (P_5 - P_4) \times P \quad \text{Eq. 2}$$

$$T = S \times P \quad \text{Eq. 3}$$

On the nominal model the exact coordinates of the datum points are known. A series of iterative techniques which are described in section 4 are used to estimate the location of the equivalent datum points on the forged model. The datum planes ***P'***, ***S'*** and ***T'*** on the forged model, shown in Figure 2, are established using Eq. 1 - Eq. 3.

After establishing the coordinates of the datum points and the datum plane normal vectors on both the nominal and forged models, a registration approach similar to that employed by the coordinate measurement technique adopted by Hsu *et al* [2] is implemented. This approach uses an iterative algorithm incorporating virtual coordinate measurement and a coordinate upgrading procedure to align the nominal datum reference frame known as the design coordinate system (DCS) with the datum reference frame of the forged model, known as the measurement coordinate system (MCS) to within a given tolerance. Both reference frames are shown in Figure 2.

The ICP approach employed by the inspection system uses a nearest neighbour algorithm based on a binary search tree to locate the corresponding points on the forged model for each point on the nominal model, as shown in Figures 3(a) and (b), respectively. A transformation matrix is generated for the measured point cloud using a least squares minimisation approach described in Section 4. The process of locating corresponding points and generating a transformation matrix between the respective point sets continues until a convergence criterion, based on the change in residual error between successive iterations, is satisfied. At this point the forged model is successfully registered in relation to the nominal model, as shown in Figure 3(c).

3.2 Measurement Data Generation and Evaluation of Geometric Parameters

Measurement data is generated at three locations on the concave and convex surfaces of the virtual blade model by intersecting the finite element mesh with a plane orthogonal to the longitudinal axis of

ACCEPTED MANUSCRIPT

the blade at the appropriate position. Sectional profiles are generated at the root, mid and tip positions on both surfaces of the blade. Figure 4 shows measurement profiles on the concave surface of a blade model.

The geometric parameters assessed are aerofoil section thickness, angular displacement of the mid and tip section also known as "twist" and vertical displacement of the mid inspection section also referred to as "bow". These parameters are evaluated at reference positions known as K points that are interpolated from the nominal model. A total of six K points are defined for each aerofoil section, as shown in Figure 5.

Following industrial CMM practice, the section thickness, δ_t is defined as the Euclidean distance between opposing K points on the concave (CC) and convex (CV) blade surfaces. Overall, section thickness is measured between three sets of K points located at the leading edge, middle and trailing edge positions for each section. Therefore for each measured value of section thickness, the thickness error, δ_1 may be subsequently obtained as the difference between the actual thickness measurement, $\delta_t^{'}$ and the respective nominal thickness, δ_t. The angular displacement at the mid and tip sections, δ_2, also known as twist error, is quantified as the angular variation from the nominal when measured at K_1 and K_5. Finally, the vertical displacement of the mid section, otherwise known as bow error, δ_3, is defined as the vertical deviation from the nominal when measured at K_3. The bow error may be calculated by the difference between y coordinate of K_3 on the nominal and measured profiles, respectively. Table 1 describes how the geometric parameters are assessed.

The total deviation between the measured profile and the nominal curve, known as form or profile error is evaluated using a least squares based approach described in Section 4. Similar approaches have been reported by Pahk *et al* [16] and Hsu *et al* [2], both of which employ the iterative closest point technique, whereby the corresponding points were generated using the Tschebyscheff norm and the Powell method, respectively. The measurement data positioning algorithm is reported in Section 4.3. Overall, six profiles are evaluated, comprising the concave and convex profile of each blade section. The form error is then calculated as the vertical deviation between the respective profiles. The form error may be represented graphically as a plot displaying the error as the deviation from the nominal profile, as shown in Figure 6.

Form tolerances are often represented by offset zones, as depicted in Figure 6. These zones are created by offsetting the nominal profile of a part by an amount equal to the tolerance on either side of the nominal. In this case, offsets are obtained for the maximum material condition (MMC) and the

ACCEPTED MANUSCRIPT

least material condition (LMC). The tolerance zone is equal to the difference between these two zones and generates an envelope within which the boundary of the part must lie [18]. Thus, the profile tolerance, t comprises the sum of two intermediate tolerances, t^+ and t^-. Hence at a given point on the nominal profile P_N, the intermediate tolerances represent the amount of tolerance allowed in the positive and negative directions of a given unit vector $\hat{V}$ (usually in y direction). Therefore, a surface conforms to a profile tolerance if each point on the measured profile, P_S lies within the intermediate tolerances disposed about some corresponding point P_N on the nominal profile. This conformance criterion may be represented using

$$P_S = P_N + \hat{V}u \qquad \text{Eq. 4}$$

where $-t^- \leq u \leq t^+$. In the example shown in Figure 6, this condition is satisfied as the error does not fall outside the offset zone.

4. Theoretical Formulation and Methodology

A mathematical description of the methods and computational procedures for part localisation, measurement data acquisition and blade parameters analysis are reported in detail in this section.

4.1 3-2-1 Registration Algorithm

To initiate localisation, datum points were firstly identified on the blade formed from the finite element forging simulation. As the initial position of the blade was in close proximity to the nominal coordinate system due to constraints applied in the FE simulation, no preliminary transformation process was required. Consider (X', Y', Z') as the measurement coordinate system and (X, Y, Z) as the design coordinate system. Consequently, P_1 - P_6 represent the nominal datum points and P_1' - P_6' represent their counterparts in the MCS. Firstly, an initial measurement of the three datum points on the aerofoil surface, P_1', P_2' and P_3' are made using a series of measurement vectors known as "back-off directions". Each measurement vector and corresponding target point is represented in the following measurement matrix

$$V = [xyzijk]^T \qquad \text{Eq. 5}$$

ACCEPTED MANUSCRIPT

where x, y and z represent the coordinate values of the target point and i, j and k represent the components of the vector which are aligned with the Y axis for the measurement of P_1', P_2' and P_3' and the z axis for P_6'. Each measurement point is calculated by determining the intersection point between the measurement vector passing through the target point and the facet it intersects on the mesh of the forged blade. Figure 7 displays the initial measurement process. The normal of the primary datum plane, ***P'*** is defined using Eq. 1. For subsequent iterations of the 3-2-1 method, the measurement vector is then approximated as the normal of the closest facet to each target. The actual coordinate measurement process follows the same procedure. After an initial registration of the blade, because the freeform surface is irregular it is necessary to obtain a more accurate indication of the measurement vector. Consequently, a local calculation of the surface normal is made by measuring three points around the target point.

Subsequently, after gaining an initial estimate of the three primary datum points, using the rules of orthogonality and sequence for datum frame construction [6], the secondary datum, perpendicular to the primary datum, is established next using the cylindrical datum reference features at the tip pip and root pip of the forging, Figure 8(a). Thus, in both the experimental CMM measurements and in the virtual inspection procedure outlined here, the known cylindrical form of the root and tip pips is used to localise and orient the aerofoil surface.

It should be noted that the axes of these cylindrical reference features are not designed to be co-linear. However, by locating a point on the axis of each cylindrical feature, it is possible to define a line (or direction vector) on the secondary datum plane. The normal of the secondary datum plane can be determined according to Eq. 2. Each secondary datum point is determined by fitting the nodal coordinates on the feature surface according to a least squares principle.

As shown in Figure 8(b) for a cylinder defined by a point on its axis $X_0 = (x_0, y_0, z_0)$, a vector along its axis $a = (a, b, c)$ and radius r, an initial estimate of these parameters may be obtained by minimising the distance function between the cylinder to m points $X_i = (x_i, y_i, z_i)$ $(m \geq 5)$, i.e.

$$d_i = r_i - r \qquad \text{Eq. 6}$$

where:

$$r_i = \frac{\left(u_i^2 + v_i^2 + w_i^2\right)^{0.5}}{\left(a^2 + b^2 + c^2\right)^{0.5}} \quad \text{Eq. 7}$$

with

$$\begin{aligned} u_i &= c(y_i - y_0) - b(z_i - z_0) \\ v_i &= a(z_i - z_0) - c(x_i - x_0) \\ w_i &= b(x_i - x_0) - a(y_i - y_0) \end{aligned} \quad \text{Eq. 8}$$

where r_i is the distance of the i^{th} point to the cylinder axis and $(X_i - X_0) \times a = (u_i, v_i, w_i)$ is the cross product of $(X_i - X_0)$ with a. By rotating and translating the data at the start of each iteration so that the trial best fit cylinder had a vertical axis passing through the origin [19], it was possible to define d_i as a function of five parameters x_0, y_0, a, b and r. To minimise the sum of the squared distances, the objective function may be linearised in the form as given in the following equation

$$d_i = (r_i - r) + (x_i - x_0)\frac{\partial d_i}{\partial x_0} + (y_i - y_0)\frac{\partial d_i}{\partial y_0} + (a_i - a)\frac{\partial d_i}{\partial a} + (b_i - b)\frac{\partial d_i}{\partial b} + (r_i - r)\frac{\partial d_i}{\partial r} \quad \text{Eq. 9}$$

With m points collected from either the tip or root pip cylinders, the least squares system may be obtained in the following form

$$JP = -d \quad \text{Eq. 10}$$

where J is the Jacobian matrix from the partial derivatives of Eq. 6 with respect to the five parameters given by

$$\frac{\partial d_i}{\partial x_0} = -\frac{x_i}{r_i}$$
$$\frac{\partial d_i}{\partial y_0} = -\frac{y_i}{r_i}$$
$$\frac{\partial d_i}{\partial a} = -\frac{x_i z_i}{r_i}$$
$$\frac{\partial d_i}{\partial b} = -\frac{y_i z_i}{r_i}$$
$$\frac{\partial d_i}{\partial r} = -1$$

Eq. 11

The Jacobian matrix may be obtained by

$$J = \begin{bmatrix} \frac{\partial d_1}{\partial x_0} & \frac{\partial d_1}{\partial y_0} & \frac{\partial d_1}{\partial a} & \frac{\partial d_1}{\partial b} & \frac{\partial d_1}{\partial r_0} \\ \frac{\partial d_2}{\partial x_0} & \frac{\partial d_2}{\partial y_0} & \frac{\partial d_2}{\partial a} & \frac{\partial d_2}{\partial b} & \frac{\partial d_2}{\partial r_0} \\ \vdots & \vdots & \vdots & \vdots & \vdots \\ \frac{\partial d_n}{\partial x_0} & \frac{\partial d_n}{\partial y_0} & \frac{\partial d_n}{\partial a} & \frac{\partial d_n}{\partial b} & \frac{\partial d_n}{\partial r_0} \end{bmatrix} = \begin{bmatrix} \frac{-x_1}{r_1} & \frac{-y_1}{r_1} & \frac{-x_1 z_1}{r_1} & \frac{-y_1 z_1}{r_1} & -1 \\ \frac{-x_2}{r_2} & \frac{-y_2}{r_2} & \frac{-x_2 z_2}{r_2} & \frac{-y_2 z_2}{r_2} & -1 \\ \vdots & \vdots & \vdots & \vdots & \vdots \\ \frac{-x_n}{r_n} & \frac{-y_n}{r_n} & \frac{-x_n z_n}{r_n} & \frac{-y_n z_n}{r_n} & -1 \end{bmatrix}$$

Eq. 12

The vector of corrections to the cylinder parameters P is be given by

$$P = \begin{bmatrix} p_{x_0} & p_{y_0} & p_a & p_b & p_r \end{bmatrix}^T$$

Eq. 13

and the distance error vector d is

$$d = \begin{bmatrix} d_1 & \cdots & d_i & \cdots & d_n \end{bmatrix}^T$$

Eq. 14

Thus, given initial estimates of the axis point, axis direction and radius, a Gauss-Newton strategy was implemented to find the solution for best fit of the tip and root pip cylinders. The detailed iteration procedure is given in [19] with the following main steps: (i) translate the point $X_0 = (x_0, y_0, z_0)$ to the centre of the origin; (ii) transform the directional vector $a = (a, b, c)$ by rotation in line with the z axis; (iii) calculate both the left and right hand sides of the least squares system, Eq. 10; (iv) solve the least squares system using the Gauss-Newton method until the convergence criterion is met. As the FE simulation of the forging process ensures close proximity of the forged blade to the nominal coordinate system, the Gauss-Newton method was found to be effective in computing iterations.

ACCEPTED MANUSCRIPT

However, in order to fit the nodal coordinates, it is necessary to identify the nodes that are situated on the surface of the cylindrical pips. Thus, a shape recognition algorithm which uses the least squares cylinder approach is employed for this purpose. To reduce processing time and simplify the search for nodes which belong to the candidate shape a 2D boundary is defined in the approximate location of the tip pip and subsequently, a second boundary is defined for the root pip. For each exposed element face within the boundary at least ten of the closest nodes are located and fitted to the candidate cylinder. If the least squares algorithm does not converge or the calculated radius exceeds the nominal radius tolerance the node set is not included in the candidate point cloud. This process continues until all exposed elements within each boundary have been evaluated. After identifying the respective point clouds each dataset is submitted to the least squares calculation which yields the coordinates of the points P_4' and P_5' on the respective cylinder axes. An example of the cylindrical point clouds generated from the searching algorithm is shown in Figure 8(a).

According to the sequence rule in datum setting, the first stage of the localisation involves aligning the components primary datum plane with that of the nominal. This may be achieved by aligning P with ***P'***, the direction cosine of the primary datum in the DCS defined in Figure 1. All rotations and translations involved in the localisation process are performed using an approach for transformation about an arbitrary plane in 3-dimensional space. This first transformation to align the primary datum plane shown in Figure 2 is composed of a translation and two rotations in sequence. After applying an initial translation to the blade to align P_1' with its counterpart on the nominal, the component is rotated by an angle θ, about the axis defined by the cross product of $\vec{P_1'P_2'}$ and $\vec{P_1P_2}$. The final rotation to align P with ***P'*** is applied around the axis defined by $\vec{P_1P_2}$. In this instance, the angle of rotation, α, is defined as the angle between the primary datum plane normals which may be calculated as the angle between ***P'*** and P. Thus, if $X_m = (x_m, y_m, z_m)$ is an arbitrary point on the surface of the blade, then the new position after the above transformation is applied can be expressed in matrix form as:

$$X'_m = X_m + T_1 \qquad \text{Eq. 15}$$

$$X_1 = R(\theta, \alpha) X'_m \qquad \text{Eq. 16}$$

where X_m is the initial position of the point on the unregistered part, X'_m is the position of the point after the translation, T_1 is the initial translation to align P_1' with P_1 and $R(\theta, \alpha)$ is rotational matrix

ACCEPTED MANUSCRIPT

for angles θ and α about their respective axes. The second phase of the localisation process involves the alignment of the blades secondary datum plane with that of the nominal. The plane is aligned by rotation about an axis defined by the primary datum normal vector at the point of intersection between the two secondary datum planes, assuming they are not parallel, as shown in Figure 2. The angle of rotation, β, is defined as the angle between S and S'. Subsequently, after the second alignment the new position of the measurement points is defined by:

$$X_2 = R(\beta)X_1 = R(\beta)R(\theta,\alpha)X'_m \qquad \text{Eq. 17}$$

The final stage to align the tertiary datum planes involves a single translation between the two coordinate frames. The translation values are found by implementing an algorithm to find the intersection point of a line projected in the direction T from the nominal P_6 point with an element face on the root block of the blade. On applying the final translation, the final position of the measurement points becomes:

$$X_3 = X_2 + T_2 = R(\beta)R(\theta,\alpha)X'_m + T_2 \qquad \text{Eq. 18}$$

where $T_2 = (t_p, t_s, t_t)$ represents translational values in the primary, secondary and tertiary planes, respectively. After the initial registration of the component, the localisation process is repeated until the discrepancy between the datum points on the blade and the corresponding points on the nominal are within the specified tolerance.

4.2 Iterative Closest Point (ICP) Localisation

The most important and computationally demanding step of an ICP algorithm involves finding the corresponding points on the reference surface. The previously mentioned ICP registration methods [2, 10] used a parametric surface representation of the design model to locate the closest points. This study uses point sets to represent the geometric data of the respective measured and nominal models, so a different technique is required to determine the corresponding points. One option is to conduct a linear search for the closest point in the nominal model to each measured point based on Euclidian distance, but for large point sets this approach is impractical as it leads to excessive computing times. The computational efficiency may be improved by as much two orders of magnitude by building a k-dimensional binary search tree or k-d tree from the data points in the nominal model and querying the tree for each point in the measured model [20]. A nearest neighbour algorithm is used to find the closest point to a given target point on the tree. At each stage of the search the algorithm makes an approximation of the nearest distance and subsequently terminates when the possibility of more than

ACCEPTED MANUSCRIPT

one nearest neighbour no longer exists [21]. Consequently, large portions of the search space can be avoided using this method.

4.2.1 Least Squares Minimisation

There are two general methods for least squares minimisation in 3D registration problems, i.e., quaternion based and singular value decomposition (SVD) based methods. Horn *et al* presented a quaternion based approach, whereby rotations were represented as quaternions to simplify problems due to orthogonal rotation matrices [22]. Alternatively, the SVD approach is computationally very efficient and easily generalised to 3D problems. Consequently, this study employs a SVD-based solution method similar to that proposed by Arun *et al* [23]. The transformation matrix generated from the least squares minimisation of the respective point sets will be represented by an orthogonal rotation matrix and a translation vector. Thus, for known correspondences between a measured point set, M_i and a nominal point set, N_i, the registration method aims to find a rotation matrix, R and a translation matrix, T that minimises the weighted sum of the squared distances between the respective point sets, given by the cost function defined in the following equation:

$$F = \sum_{i}^{S} w_i \| N_i - (RM_i + T) \|^2 \qquad \text{Eq. 19}$$

where S represents the size of the measured point set and the weights $w_i = 1/S$. Given that R is an orthonormal rotation matrix, then $R^T = R^{-1}$. Thus, if the rotation matrix is represented by

$$R = \begin{bmatrix} r_1^T \\ r_2^T \\ r_3^T \end{bmatrix} \qquad \text{Eq. 20}$$

where each component of R is a 3 x 1 vector, the orthogonality constraint results in the following six constraint equations:

$$\begin{aligned} r_1^T r_1 &= 1 \\ r_2^T r_2 &= 1 \\ r_3^T r_3 &= 1 \\ r_1^T r_2 &= 0 \\ r_1^T r_3 &= 0 \\ r_2^T r_3 &= 0 \end{aligned} \qquad \text{Eq. 21}$$

Applying these constraints, Eq. 19 may be represented as

$$F = \sum_{i=1}^{S}\sum_{k=1}^{3} w_i\left(N_{ik} - r_k^T M_i - T_k\right)^2 + \sum_{k=1}^{3}\lambda_k\left(r_k^T r_k - 1\right) + 2\lambda_4 r_1^T r_2 + 2\lambda_5 r_1^T r_3 + 2\lambda_6 r_2^T r_3 \quad \text{Eq. 22}$$

where λ_i, i=1-6 represent Lagrangian multipliers used to enforce the orthogonality constraints and

$$N_i = \begin{bmatrix} N_{i1} \\ N_{i2} \\ N_{i3} \end{bmatrix},\ M_i = \begin{bmatrix} M_{i1} \\ M_{i2} \\ M_{i3} \end{bmatrix} \text{ and } T = \begin{bmatrix} T_1 \\ T_2 \\ T_3 \end{bmatrix} \quad \text{Eq. 23}$$

As is detailed in Arun *et al* [23], the minimisation condition may then be applied by equating the partial derivative of F with respect to λ_j to zero, resulting in

$$\sum_{i-1}^{S} w_i\left(N_i - RM_i - T\right) = 0 \quad \text{Eq. 24}$$

Rearranging Eq. 24 gives

$$T = \overline{N} - R\overline{M} \quad \text{Eq. 25}$$

where the centroids of the nominal and measured point sets may be calculated according to:

$$\overline{N} = \frac{\sum_{i=1}^{S} w_i N_i}{\sum_{i=1}^{S} w_i} \quad \text{and} \quad \overline{M} = \frac{\sum_{i=1}^{S} w_i M_i}{\sum_{i=1}^{S} w_i} \quad \text{Eq. 26}$$

Thus, on substitution of Eq. 26 into Eq. 22, F may be defined as

$$F = \sum_{i=1}^{S} w_i \sum_{k=1}^{3}\left(N_{ik} - \overline{N}_k - r_k^T\left(M_i - \overline{M}\right)\right)^2 + \sum_{k=1}^{3}\lambda_k\left(r_k^T r_k - 1\right) + 2\lambda_4 r_1^T r_2 + 2\lambda_5 r_1^T r_3 + 2\lambda_6 r_2^T r_3 \quad \text{Eq. 27}$$

By equating the partial derivative of F with respect to the components of r_j to zero yields the following series of equations

$$\sum_{i=1}^{S} w_i\left(M_i - \overline{M}\right)\left(M_i - \overline{M}\right)^T r_1 + \lambda_1 r_1 + \lambda_4 r_2 + \lambda_5 r_3 = \sum_{i=1}^{S} w_i\left(N_{i1} - \overline{N}_1\right)\left(M_i - \overline{M}\right) \quad \text{Eq. 28}$$

$$\sum_{i=1}^{S} w_i\left(M_i-\overline{M}\right)\left(M_i-\overline{M}\right)^T r_2+\lambda_4 r_1+\lambda_2 r_2+\lambda_6 r_3=\sum_{i=1}^{S} w_i\left(N_{i2}-\overline{N}_2\right)\left(M_i-\overline{M}\right) \quad \text{Eq. 29}$$

$$\sum_{i=1}^{S} w_i\left(M_i-\overline{M}\right)\left(M_i-\overline{M}\right)^T r_3+\lambda_5 r_1+\lambda_6 r_2+\lambda_3 r_3=\sum_{i=1}^{S} w_i\left(N_{i3}-\overline{N}_3\right)\left(M_i-\overline{M}\right) \quad \text{Eq. 30}$$

These equations may be simplified by letting

$$A=\sum_{i=1}^{S} w_i\left(M_i-\overline{M}\right)\left(M_i-\overline{M}\right)^T \quad , \quad \Lambda=\begin{bmatrix}\lambda_1 & \lambda_4 & \lambda_5\\ \lambda_4 & \lambda_2 & \lambda_6\\ \lambda_5 & \lambda_6 & \lambda_3\end{bmatrix} \quad , \quad B=\left[b_1 b_2 b_3\right] \quad \text{Eq. 31}$$

where

$$b_k=\sum_{i=1}^{S} w_i\left(N_{ik}-\overline{N}_k\right)\left(M_i-\overline{M}\right) \quad \text{Eq. 32}$$

Thus, Eq. 28 – Eq. 30 may be represented as

$$AR^T+R^T\Lambda=B \quad \text{Eq. 33}$$

Multiplying both sides of Eq. 33 by R gives

$$RAR^T+\Lambda=RB \quad \text{Eq. 34}$$

Consequently, R may be found by obtaining the singular value decomposition of B, whereby

$$B=UDV \quad \text{Eq. 35}$$

Since both RAR^T and Λ are symmetric, Eq. 33 implies

$$RB=\left(RB\right)^T \quad \text{Eq. 36}$$

Therefore

$$RUDV=\left(UDV\right)^T R^T \quad \text{Eq. 37}$$

Given that U and V are orthogonal and D is diagonal, then

$$R=V^T U^T \quad \text{Eq. 38}$$

Thus, once R is known, T is determined using Eq. 25.

ACCEPTED MANUSCRIPT

4.2.2 The ICP Algorithm

The main limitation with the ICP method is that the presence of local minima within the parameter space explored by the algorithm may lead to non-global convergence. However, this scenario can be avoided by ensuring that the respective surfaces are located in close proximity before applying ICP, thereby providing a greater chance of convergence to the global minimum. In any case, for the purposes of this study, due to the constraints applied in the FE simulation, the respective models are sufficiently close to implement the ICP algorithm. The ICP algorithm implemented in this study consists of the following steps:

(i) For each discrete point, M_i in the measured point set compute the closest point (in terms of Euclidean distance), N_i on the surface of the nominal model.

(ii) Calculate the rotation matrix, R and translation matrix, T which minimises the cost function defined by Eq. 25 using the SVD-based solution method.

(iii) Apply the transformation to the measured point set.

(iv) If the change in residual error from Eq. 25 is greater than a threshold value, go back to step (i); otherwise stop.

Convergence to a minimum is found by comparing the change in residual error between iterations with a pre-specified threshold value. Local minima are detected if a significant number of residuals are above the threshold. In this case, the ICP procedure is set to terminate when the difference in residual error is less then $1e^{-5}$.

4.3 Blade Profile Positioning for Profile Error Evaluation

After localisation, there remains a total deviation between the measured profile and the nominal curve. Therefore, this necessitates an algorithm to align the respective data sets in order to gain an accurate appraisal of the profile error. The profile error evaluation algorithm employed by the virtual inspection system aligns the concave and convex profiles of each section with their counterparts on the nominal at predefined locations specified by the K points close to the leading (K_1 and K_2) and trailing (K_5 and K_6) edges of the nominal model. This repositioning procedure is implemented by performing a translation, T and rotation, R in sequence. Firstly, each measured profile is translated vertically until it coincides with the relevant nominal profile at K_1 or K_2. The second stage of the transformation involves alignment with the remaining K point at K_5 or K_6. This is achieved by rotation about K_1 or K_2. However, in order to find the required angle of rotation, it is necessary to use a

ACCEPTED MANUSCRIPT

searching algorithm to locate a direction vector $K_1'\vec{K}'_{prof}$ on the measured profile with a magnitude equal to $\left|K_1'\vec{K}_5\right|$. K'_{prof} is the point on the measured profile located by the searching algorithm.

The blade profile positioning and error evaluation process for a concave profile is described in the following steps:

(i) Apply a translation, T to the measurement profile, D_m to coincide with K_1. Thus, if $P_S = (x_S, y_S)$ is an arbitrary point on the concave blade profile, then the new position, P'_S after the above transformation is applied can be expressed in matrix form as:

$$P'_S = P_S + T \qquad \text{Eq. 39}$$

(ii) Search through the repositioned measurement data for the point K'_{prof} such that

$$\left|K_1'\vec{K}_5\right| = \left|K_1\vec{K}'_{prof}\right| \qquad \text{Eq. 40}$$

(iii) Apply a rotation, R to the repositioned measurement data by an amount φ defined by

$$\phi = \cos^{-1}\left(\frac{K_1'\vec{K}_5 \cdot K_1\vec{K}'_{prof}}{\left|K_1'\vec{K}_5\right|\left|K_1\vec{K}'_{prof}\right|}\right) \qquad \text{Eq. 41}$$

Consequently, the newly positioned measurement data, D'_m is defined by

$$D'_m = T + R(\varphi)D_m \qquad \text{Eq. 42}$$

(iv) Produce a graphical plot displaying the form error as the deviation of the newly positioned measured profile from the nominal profile, as shown in Figure 6.

5. System Framework

The virtual inspection systems software framework is based on an object-orientated design, which operates on a Windows platform. The open source, high level programming language, Python, forms the core of the scripting architecture. Python is ideally suited to this application for a variety of reasons including its diverse library of standard extensions, in particular the Numpy extension which allows the efficient storage and manipulation of substantial amounts of numerical data, its modularity and it offers extensibility, permitting the extension of existing programs with modules for implementing specific functionality. As some of the aforementioned least squares calculations and

ACCEPTED MANUSCRIPT

form fitting algorithms are performed in Matlab, the system employs a high-level Python to Matlab bridge or application programming interface (API), which starts a Matlab engine session in the background, permitting Matlab functions to be called from Python by allowing Numpy arrays to be passed back and forth and arbitrary commands to be executed in the Matlab workspace.

The finite element forging simulation was conducted using DEFORM-3D. The entire virtual inspection system framework is composed of five layers. The data input layer comprises three components including the nominal model in *.stl* format, the model of the forged blade in either *.key* (native DEFORM-3D format) or *.stl* format and a *.txt* file detailing the user defined input parameters. Primarily, the input parameter file consists of nominal coordinate data for the K points and the six datum points that define design coordinate frame. Other parameters specified include tolerance values for the convergence criteria used by the various iterative algorithms employed by the system. Also, file paths are designated, defining the location of the respective input blade models and an appropriate folder to store the results of the parameters analysis module. Figure 9 shows the framework of the entire virtual inspection system.

6. Results and Discussion

To illustrate the effectiveness of the proposed methodology, a test case of a forged compressor blade is presented in this section. All relative geometric and dimensional tolerances of the finite element model are evaluated by the virtual inspection system and a comparison is made with inspection data from the actual component.

6.1 Finite Element Simulation

A finite element forging simulation of an industrial case Ni-alloy blade was performed. The constitutive models defining the deformation behaviour for the billet were defined as rigid-plastic during forging and elastic-plastic during the unloading and cooling stages, whereas elastic deformation was defined for the forging dies throughout the entire simulation. Figure 10 displays the meshed 3D models of the components used in the forging simulation.

The initial temperatures specified for the billet and the dies were 1000 ˚C and 230 ˚C, respectively. Other parameters defined in the pre-processing environment include the heat transfer coefficient at the interface between the workpiece and dies, h_f which was set at 11 kW/m^{2o}C and the coefficient of friction, μ between the workpiece and die surface which was assumed to be 0.2 [5, 24]. The forging simulation comprised of four stages including forging, unloading, cooling and trimming. Figure 11 shows the FE model including both the dies and workpiece before and after forging operations.

ACCEPTED MANUSCRIPT

6.2 Profile Error Evaluation

To assess the accuracy of the blades formed from the finite element method, a comparison is made between the actual profile error recorded by the coordinate measurement process and that generated by the virtual inspection system. A one-way analysis of variance (ANOVA) test is used to test for differences between the CMM and virtual profile error data sets. The *.stl* file of the designed aerofoil blade, also used as the geometry for generating the FE meshes of the forging dies, are used as blade nominal shape, whilst the nodal positions of the FE mesh from the final forged aerofoil shape excluding the flash areas are used for finding the datum features in the 3-2-1 registration method and for generating the point cloud using the ICP method. Table 2 details a comparison between the profile error recorded by the coordinate measurement machine and the virtual inspection system. As variants are both positive and negative for the profile error, the root mean square (RMS) error is the most appropriate representation of the average deviation from the nominal. Also, the standard deviation and p value are recorded for the each data set.

The virtual inspection and corresponding CMM profile error plots are shown in Figures 12 to 23. It should be noted that the vertical axis on these plots refers only to the definition of the nominal profile (highlighted in blue). The actual error and tolerance bands (defined in black and red respectively) are scaled up by a factor of 10. This is indicated in the top left of each error plot. The profile error at the mid convex section displays the strongest correlation with a comparatively large p value of 0.741. This strong comparison is further reaffirmed by the high degree of similarity apparent between the form of the profile error plots, evident in Figures 14 and 15. Overall, a good level of conformity exists between the respective profile error plots with the vast majority of cases reporting p values in excess of 0.05 and thereby failing to reject the null hypothesis, indicating no apparent statistical significant difference between the respective datasets. The only exception to this trend applies to the root concave profile. As indicated by the results of the ANOVA test, a significant level of divergence is noticeable between the CMM and virtual measurements, particularly around the trailing edge region of the profile, as shown in Figure 19. This occurrence may be attributed to the inaccuracy of the FE simulation in the transition area close to the root block due to a relatively coarse mesh.

6.3 Comparison of Dimensional and Geometric Tolerances

The dimensional and geometric tolerance measurements performed by the comparative analysis module of the virtual inspection system, as well as a comparison with the corresponding CMM data are given in Tables 3-5.

In terms of the thickness data, it is evident from Table 3 that a strong correlation exists between the virtual and CMM measurements as similar values of section thickness and standard deviation are

ACCEPTED MANUSCRIPT

recorded. Also, relatively small discrepancies between the inspection processes are apparent for bow error measurements. Moreover, as shown in Table 4, a similar trend in the magnitude of the bow error is apparent, as in each case the maximum bow occurs at the root section. However, in terms of twist error as shown Table 5, the average value recorded from the final model is roughly three times the magnitude of that recorded by the CMM. Moreover, the CMM data indicates a change in twist angle direction between the mid and tip section, whereas the twist angle remains in the same direction for the forged finite element model. This occurrence may be related to inaccuracies in post-forging simulation.

6.4 Evaluation of Localisation Methods

The virtual inspection system offers two forms of localisation, namely the *3-2-1* method which incorporates the use of datum points to register the component and the ICP method which is more suited to the registration of free-form surfaces. This section compares the effectiveness of both methods in localising the part by analysing the deviation from the nominal over the measured area of the free-form surface.

Figures 24 and 27 display the deviation of the measured area of the aerofoil surface from the nominal after localisation by the *3-2-1* and ICP methods, respectively. Accompanying the deviation contour plots are histograms indicating the frequency distribution of the deviation data and normality plots to assess the likelihood of each dataset adhering to a normal distribution.

In relation to the *3-2-1* registered model, it is obvious that the concave surface of the aerofoil exhibits a generally smaller deviation from the nominal in comparison to the convex surface. This trend may be attributed to the fact that all three of the datum points forming the primary datum plane on the model are located on the concave surface of the model. Therefore, in general, the concave surface will be positioned much closer to its counterpart surface on the nominal in comparison to the convex surface, thus yielding a comparatively smaller deviation overall. Consequently, as a result of this mismatch in the alignment of the respective free-form surfaces, the distribution of the deviation data will inevitably be affected. The shape of the distribution is revealed by the histogram of the frequency distribution in Figure 25.

The diagram indicates a bimodal or “two-peak” distribution as opposed to the classical unimodal distribution. This is characterised by the appearance of two centres or regions where most probability resides within the body of the distribution. Each of the respective regions represents the deviation data for the concave and convex surfaces. The validity of this observation may be confirmed by comparing the location of the deviation data indicated by Figure 24 in relation to the distribution of the data

ACCEPTED MANUSCRIPT

shown in Figure 25. The plot shown in Figure 26 displays a significant amount of variation from the straight line, indicating the data is obviously not normally distributed.

Conversely, as shown in Figure 27, the ICP localised surface displays a more uniform deviation with values of similar magnitude recorded for each surface. The distribution of the data, as shown in Figure 28, is relatively symmetric. Also, the majority of data points on the normality plot shown in Figure 29 form a linear pattern, indicating that the normal distribution is a good model for this data set. Suspected outliers, identified as points lying of the hypothetical straight line, are apparent towards the upper extremities of the deviation data set. These values correspond with relatively large deviation values recorded on the contour plot towards the leading and trailing edges of the root section, as shown in Figure 27. On comparing the two methods, it is clear that the ICP approach is much more effective in registering the part, as the algorithm is applied to the entire surface of the component and is not just confined to specific datum points or reference features, as with the *3-2-1* method. This serves to generate a localised part with a symmetric distribution of the deviation data and significantly less statistical dispersion, as indicated in Table 6. Although better registration accuracy may be achieved using the ICP method in virtual inspection, quantitative evaluation of the effect on the dimensional and shape accuracy of the forged blade has yet to be established, which is one area for further study. In terms of the computational efficiency of the virtual inspection, less than 100 second computing time is required for the localisation computation using a normal desktop computer. As the registration algorithm was the most computationally expensive aspect of the approach, the whole virtual inspection procedure is compared more favourably to the actual CMM measurement process, which normally takes up to 5 minutes to complete the 3-2-1 registration of the actual part.

As any deviation in the shape or form of either cylindrical datum feature would significantly affect the location of the datum reference frame, it is necessary to gain an accurate appraisal of the extent to which each cylindrical surface deviates from the desired form, implied by the nominal. An indication of the cylindrical deviation may be achieved by measuring the cylindricity of each datum feature. According to the ANSI Y14.5.1M standard [25], cylindricity is categorised as a form tolerance and is defined as "a *condition of a surface of revolution in which all points of the surface are equidistant from a common axis".* A cylindricity tolerance specifies that all points of the surface must lie in some zone bounded by two coaxial cylinders whose radii differ by the specified tolerance. The cylindricity tolerance is defined according to

$$\left\| \hat{T} \times \left(\vec{P} - \vec{A} \right) \right| - r \Big| \leq \frac{t}{2} \qquad \text{Eq. 43}$$

ACCEPTED MANUSCRIPT

where $\hat{T}$ is the direction vector of the cylindricity axis, $\vec{A}$ is a position vector locating the cylindricity axis, $\vec{P}$ is the position vector of a point on the surface of the datum feature, r is the radial distance from the cylindricity axis to the centre of the tolerance zone and t is the size of the cylindricity zone. The cylindricity for both the root and tip cylindrical datum features was evaluated for each feature using the nodal positions of the finite element mesh over each features surface. The mean cylindricity calculated for the root and tip datum features was 0.10 mm and 0.04 mm respectively with a standard deviation of 0.04 mm and 0.03 mm. By using a t value similar to that of the profile error tolerance of 0.2mm, the cylindricity value for both pips meets the specified tolerance, as defined in Eq. 43.

7. Conclusions

In terms of the localisation process, results indicate that the classical *3-2-1* approach commonly used by the CMM in industry may not be the best approach in the application to the free-form aerofoils surface. Alternatively, the ICP approach provides a much better solution to the registration problem by considerably reducing the deviation from the nominal and generating a more uniformly localised part. Overall, the magnitude and form of the profile tolerances assessed by the system display a strong correlation with that evaluated by the CMM. Virtual inspection data obtained from FE simulation recorded for the section thickness was highly consistent with the corresponding CMM data, with a discrepancy of 6 μm and 4 μm recorded for the r.m.s thickness and standard deviation, respectively. Similarly, the results generated for the bow error were also highly comparable with the actual inspection data, as the r.m.s value generated by the system differs by only 6 μm. Conversely, a relatively large deviation was apparent between the twist error values for both the mid and tip sections. This unusually large deviation in twist is likely to be attributed to the inaccuracy of the post-forging simulation, in particular, the simulation of the cooling process. However, by conducting a sensitivity analysis of the effect of pre-processing conditions such as friction and mesh density on the dimensional accuracy of the component, it may be possible to obtain inspection results which are even more consistent with the CMM data.

In any case, the virtual inspection system provides a fully automated, robust procedure for the dimensional inspection of forged aerofoil blade models formed using the finite element method. The localisation process used by the system accurately registers the component with the nominal model. The inspection and parameters analysis modules incorporate various iterative algorithms and the latest evaluation techniques to successfully quantify the forging error to within a high degree of accuracy. The strong correlation between measurements generated from this system and actual CMM measurement data, and the normal distribution of shape deviation from the nominal model, validates

ACCEPTED MANUSCRIPT

the approach as an effective means to quantify the forging error using the coordinate measurement process in a virtual environment.

8. Acknowledgements

The authors would like to thank the UK Engineering and Physical Science Research Council (EPSRC) for funding of the present research (EP/C004140/1 and EP/C004140/2).

9. References

1. Li Y, Gu P. Free-form surface inspection techniques state of the art review. *Journal of Computer-Aided Design* 2004; 36(13): 1395-1417.
2. Hsu T, Lai J, Ueng WE. On the development of airfoil section inspection and analysis technique. *International Journal of Advanced Manufacturing Technology* 2006; 36: 1-12.
3. Hartley P. *(et al)*. Numerical simulation of the forging process. *Computer Methods in Applied Mechanics & Engineering* 2006; 195(48-49): 6676-6690.
4. Bariani PF, Bruschi S and Dal Negro T. Integrating physical and numerical simulation techniques to design the hot forging process of stainless steel turbine blades, *International Journal of Machine Tools & Manufacture* 2004; 44(9): 945-951.
5. Lu B, Ou H, Armstrong C G, et al. 3D die shape optimisation for net-shape forging of aerofoil blades, *Materials & Design* 2009; 30(7): 2490-2500.
6. Hsu T, Lai J, Ueng WE, Hwang JZ. A coordinate setup algorithm based on six points principle for airfoil blades inspection. *Journal of Chinese Society of Mechanical Engineers* 2004; 25(4): 353-361.
7. Li Y, Gu P. Inspection of free-form shaped parts. *Journal of Robotics and Computer-Integrated Manufacturing* 2005; 21(3): 421-430.
8. Besl PJ, McKay ND. A method for registration of 3D shapes. *IEEE Transactions on Pattern Analysis and Machine Intelligence* 1992; 14(2): 239-256.
9. Huang X, Gu P, Zernicke R. Localisation and comparison of two free-form surfaces. *Journal of Computer-Aided Design* 1996; 28(12): 1017-1022.
10. Menq CH, Yau HT, Lai GY. Automated precision measurement of surface profile in CAD-directed inspection. *IEEE Transactions on Robotics and Automation* 1992; 8(2): 268-278.
11. Ainsworth I, Ristic M, Brujic D. CAD-based measurement path planning for free-form shapes using contact probes. *International Journal of Advanced Manufacturing Technology* 2000; 16(4): 23-31.
12. Ristic M, Brujic D, Ainsworth I. Measurement-based updating of turbine blade CAD models: a case study. *International Journal of Computer-Integrated Manufacturing* 2004; 17(4): 352-363.
13. Lai JY, Chen KJ. Localisation of parts with irregular shape for CMM inspection. *International*

ACCEPTED MANUSCRIPT

Journal of Advanced Manufacturing Technology 2007; 32: 1188-1200.

14. Hsu T, Lai J, Ueng WE, Hwang JZ. An iterative coordinate setup algorithm for airfoil blade inspection. *International Journal of Advanced Manufacturing Technology* 2005; 26(7-8): 797-807.
15. Cardew-Hall M, Cosmas J, Ristic M. Automated proof inspection of turbine blades. *International Journal of Advanced Manufacturing Technology* 1988; 3(2): 67-88.
16. Pahk HJ, Ahn WJ. Precision inspection system for aircraft parts having very thin features based on CAD/CAI integration. *International Journal of Advanced Manufacturing Technology* 1996; 12(2): 442-449.
17. Huang X, Gu P. CAD-model based inspection of sculptured surfaces with datums. *International Journal of Production Research* 1998; 36(5): 1351:1367.
18. Ge Q, Chen B, Smith P, Menq CH. Tolerance specification and comparative analysis for computer integrated dimensional inspection. *International Journal of Production Research* 1992; 30(9): 2173-2179.
19. Forbes AB. Least-squares best fit geometric elements. *National Physics Laboratory Report* 1989.
20. Bentley JL. Multidimensinal binary search trees used for associative searching. *Communications of the ACM* 1975; 18(9): 509-517.
21. Friedman JH, Bently JL, Finkel RA. An algorithm for finding best matches in logarithmic expected time. *ACM Transactions on Mathematical Software* 1977; 3(3): 209-226.
22. Horn BKP. Closed form solution of absolute orientation using unit quaternions. *Journal of the Optical Society of America A* 1987; 4(4): 629-642.
23. Arun KS, Huang TS, Blostein. Least-squares fitting of two 3D point sets. *IEEE Transactions on Pattern Analysis and Machine Intelligence* 1987; 9(5): 698-700.
24. Lu B. 3D die shape optimisation for net shape forging of aerofoil blades. *PhD Dissertation.* 2008; Queen's University, Belfast.
25. Dimensioning and Tolerancing, ANSI Standard Y14.5M. American National Standard Institute, 1994.

ACCEPTED MANUSCRIPT

ACCEPTED MANUSCRIPT

List of Figures

ACCEPTED MANUSCRIPT

ACCEPTED MANUSCRIPT

ACCEPTED MANUSCRIPT

List of Tables

ACCEPTED MANUSCRIPT

Figures&Tables

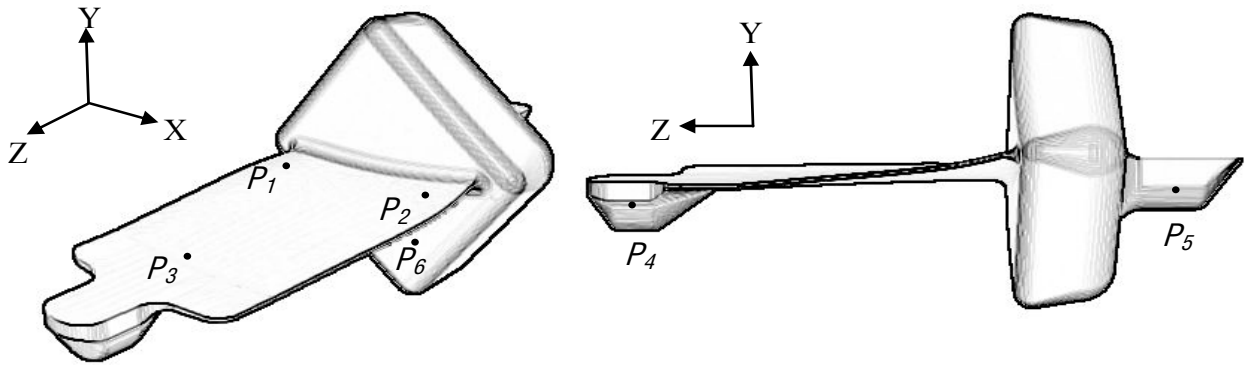

Figure 1 Datum point positions for locating the design coordinate system on the nominal model

ACCEPTED MANUSCRIPT

ACCEPTED MANUSCRIPT

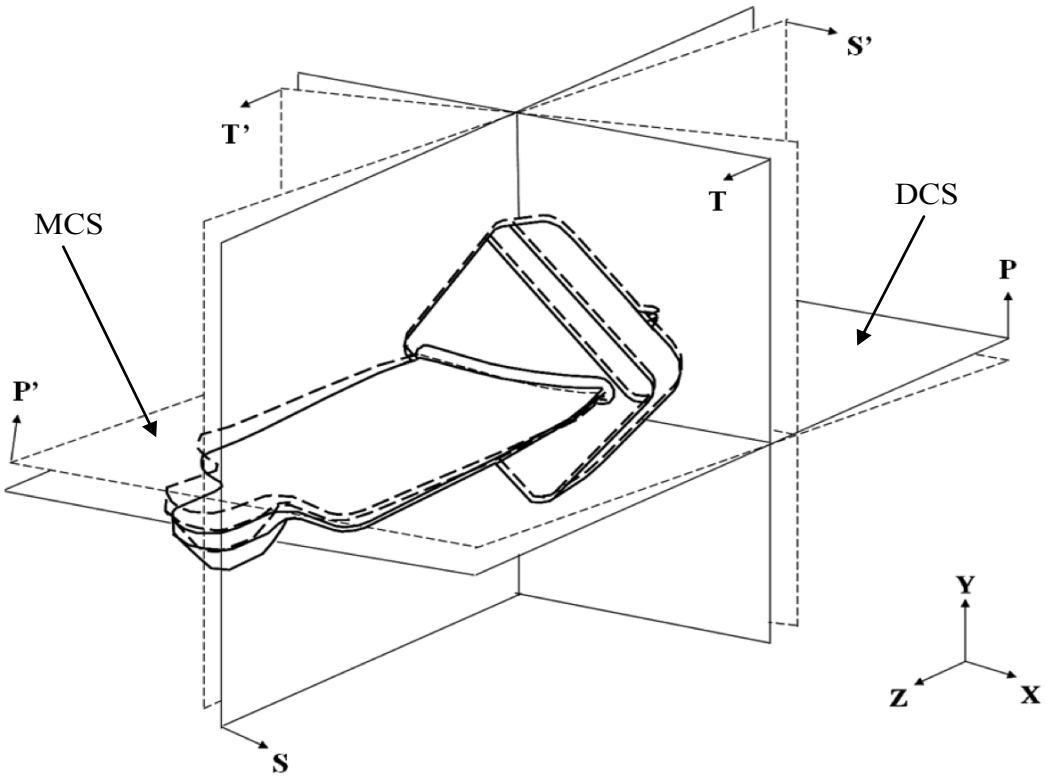

Figure 2 Respective datum planes of nominal and forged components

ACCEPTED MANUSCRIPT

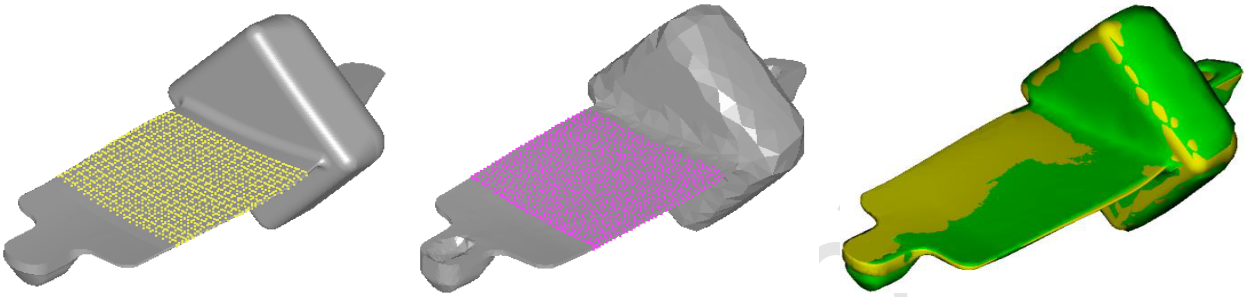

(a) Nominal model (point cloud in yellow)

(b) Forged model (point cloud in purple)

(c) Forged model (green) localised in relation to nominal model (yellow)

Figure 3 ICP localisation of a forged aeroengine blade model.

ACCEPTED MANUSCRIPT

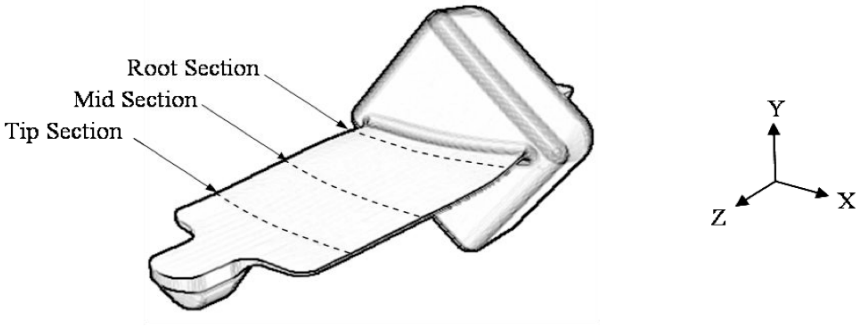

Figure 4 Location of aerofoil measurement sections

ACCEPTED MANUSCRIPT

ACCEPTED MANUSCRIPT

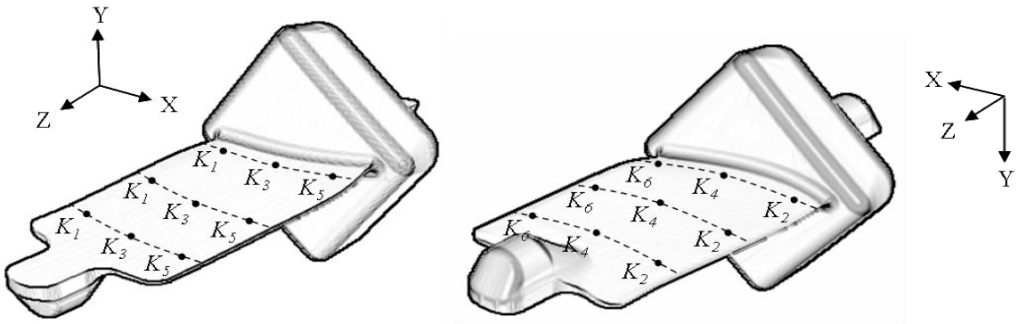

(a) Concave surface (b) Convex surface

Figure 5 K point position on concave and convex surface

ACCEPTED MANUSCRIPT

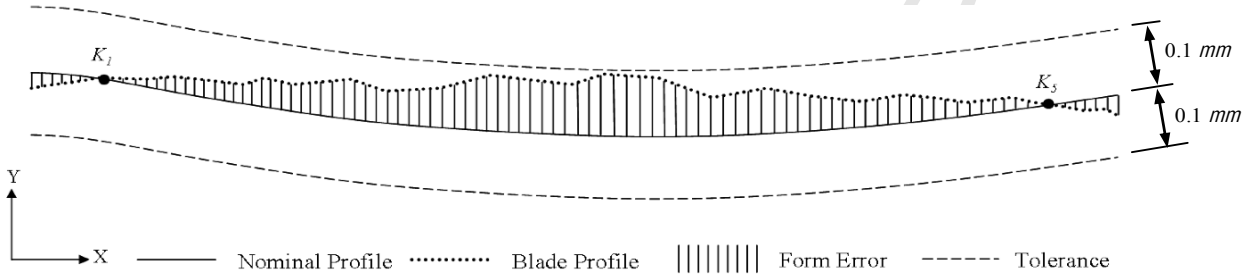

Figure 6 A plot displaying the form error of a typical concave profile

ACCEPTED MANUSCRIPT

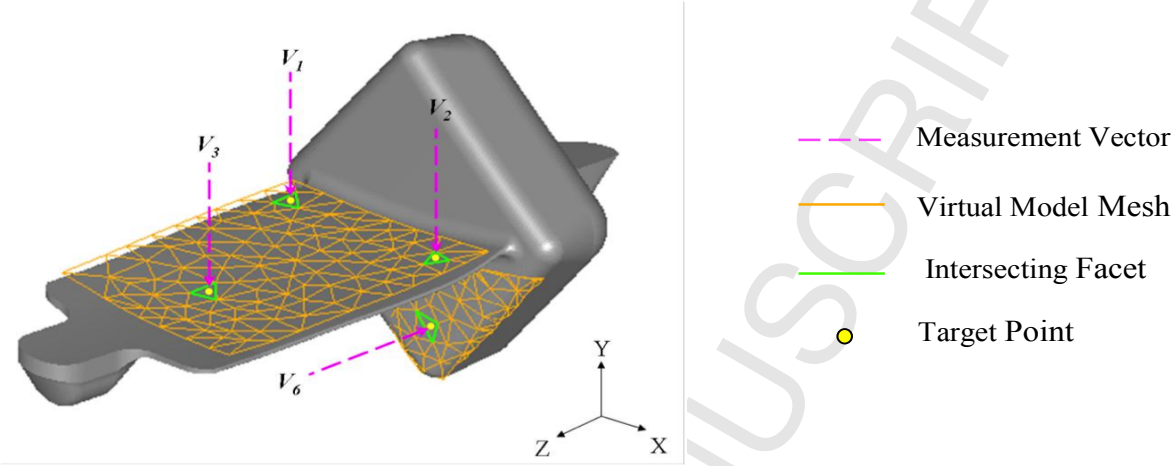

Figure 7 Datum points for initial coordinate system

ACCEPTED MANUSCRIPT

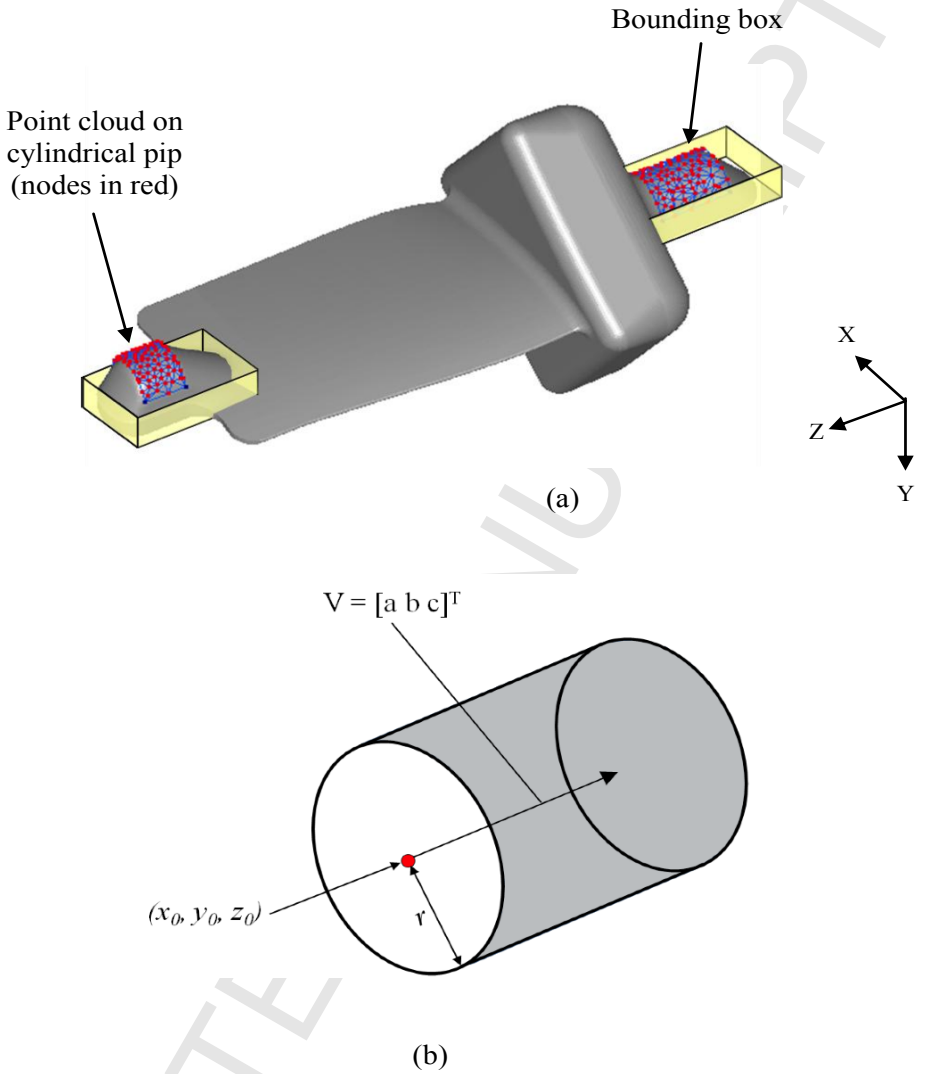

Figure 8 Cylindrical point clouds submitted for least squares calculation (Note that the root and tip pips are not co-axial)

ACCEPTED MANUSCRIPT

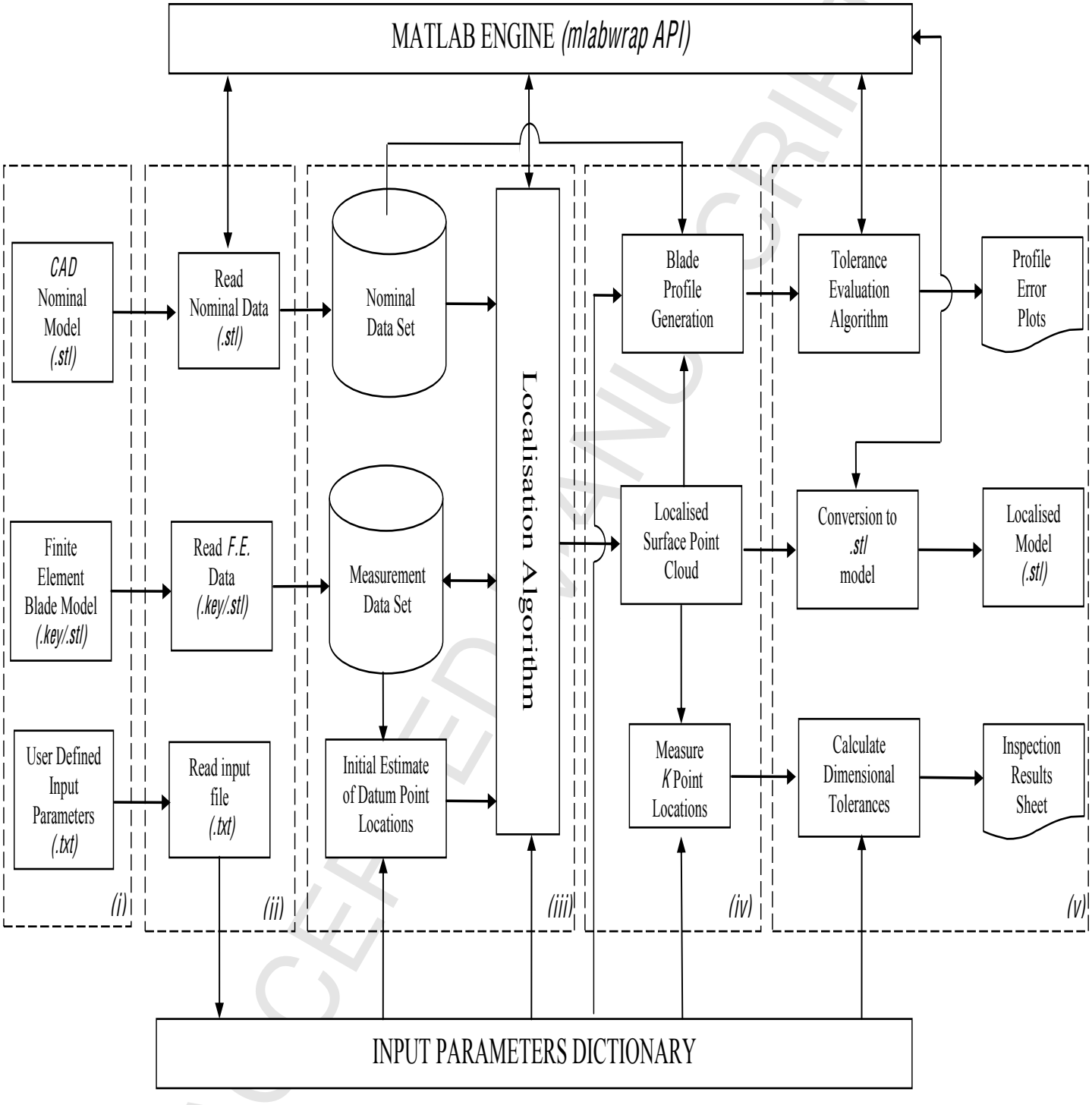

Figure 9 Virtual inspection system framework

ACCEPTED MANUSCRIPT

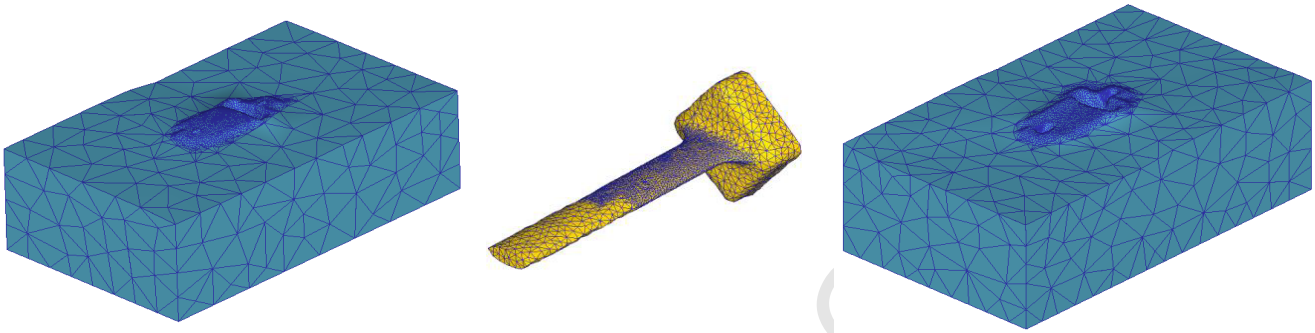

(a) Convex die (b) Workpiece (c) Concave die

Figure 10 3D model of workpiece and forging dies

ACCEPTED MANUSCRIPT

ACCEPTED MANUSCRIPT

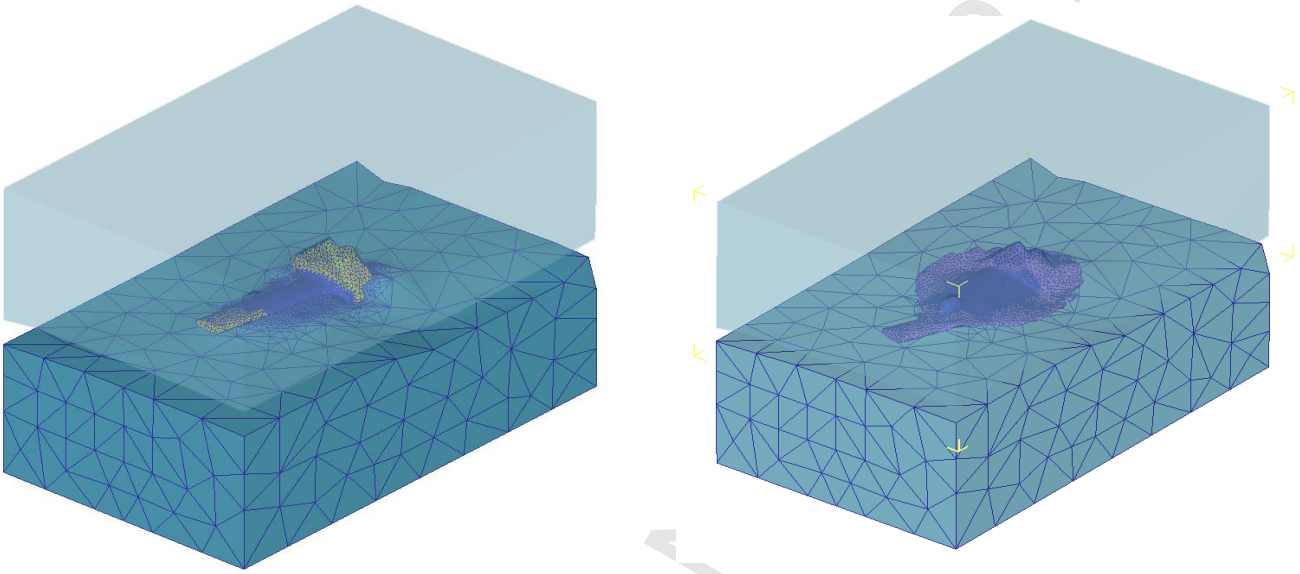

(a) Initial mesh (b) Post-cooling

Figure 11 Finite element mesh of workpiece and die

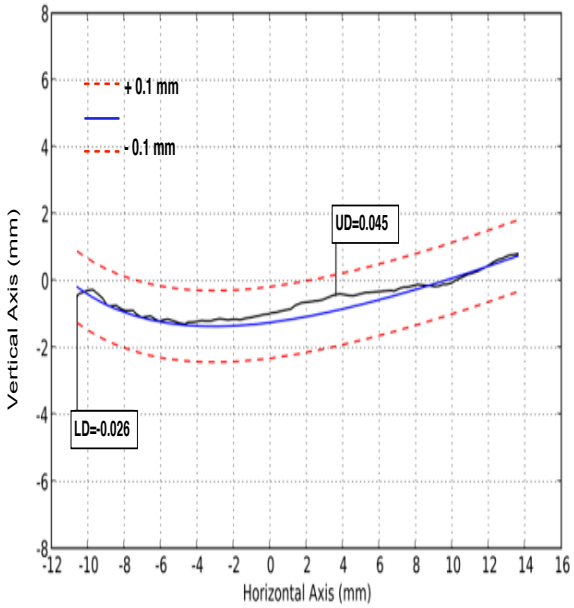

Figure 12 Virtual root convex profile error

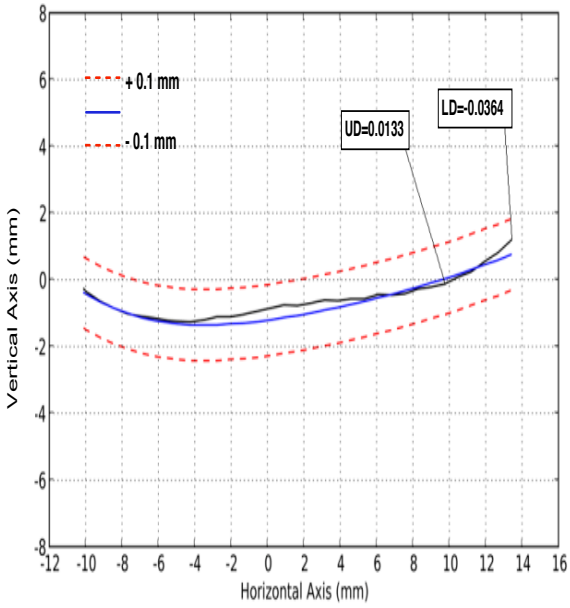

Figure 13 CMM root convex profile error

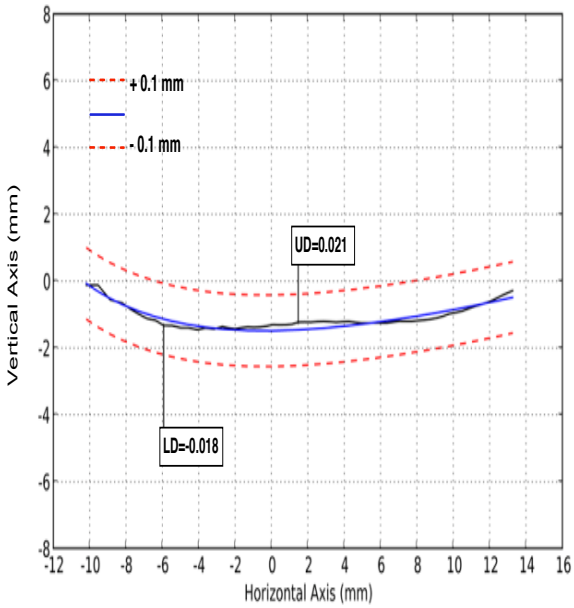

Figure 14 Virtual mid convex profile error

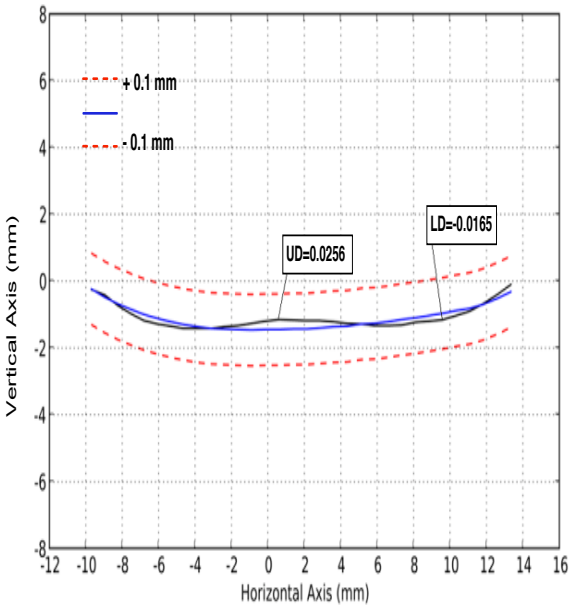

Figure 15 CMM mid convex profile error

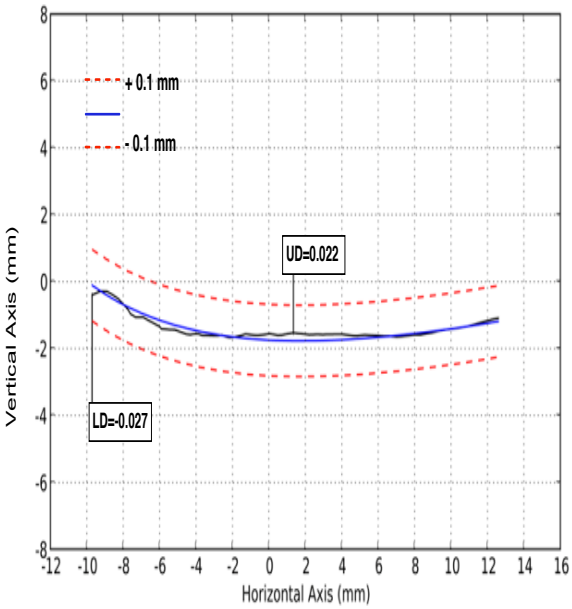

Figure 16 Virtual tip convex profile error

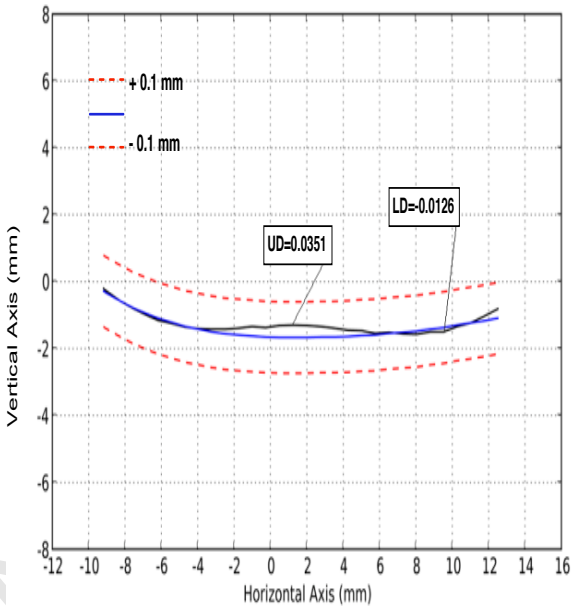

Figure 17 CMM tip convex profile error

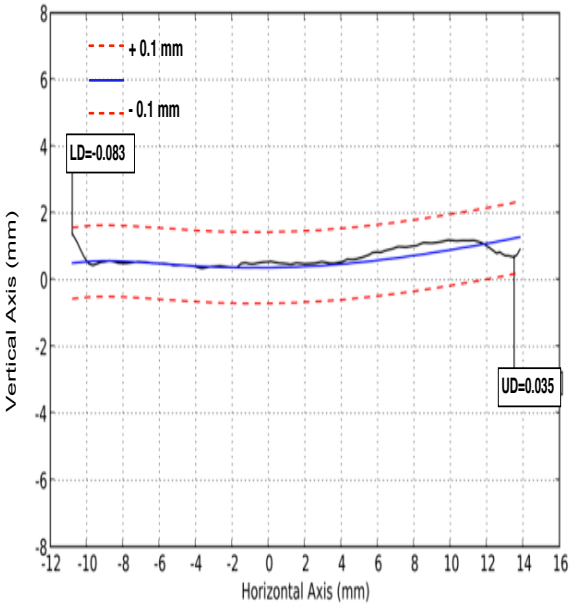

Figure 18 Virtual root concave profile error

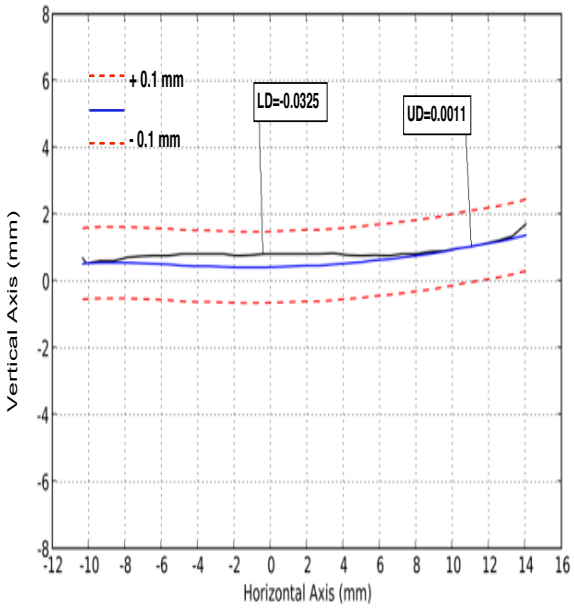

Figure 19 CMM root concave profile error

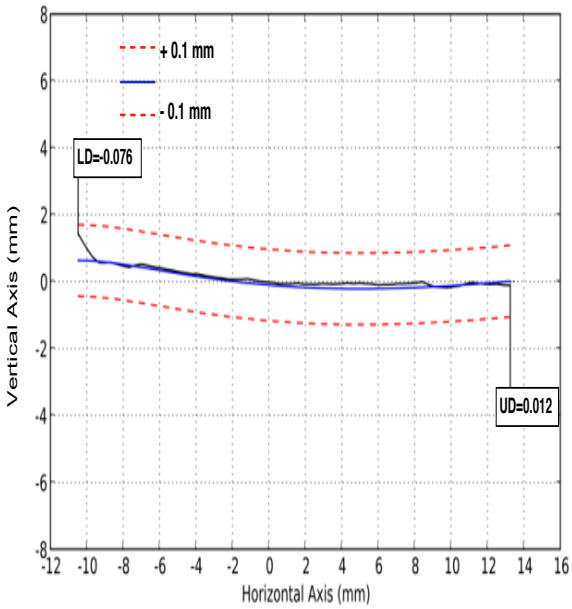

Figure 20 Virtual mid concave profile error

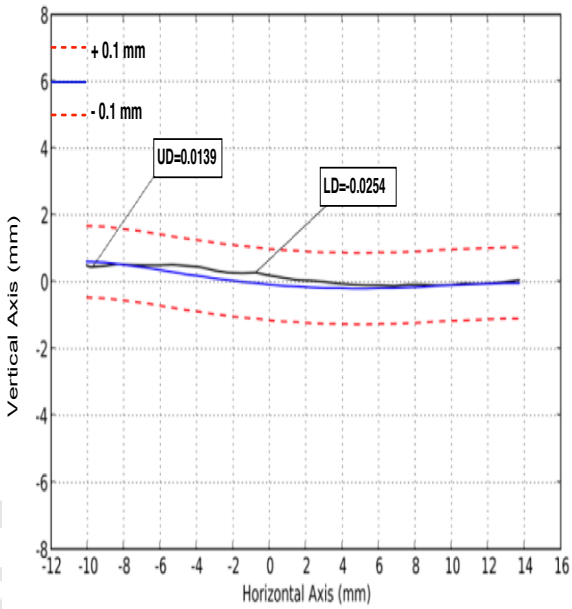

Figure 21CMM mid concave profile error

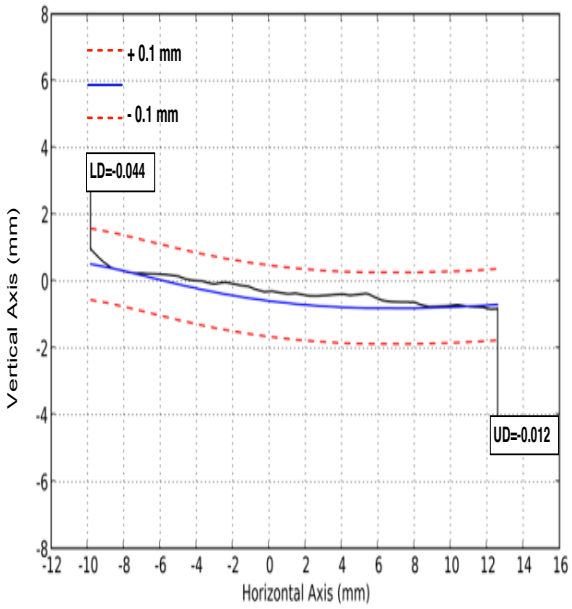

Figure 22 Virtual tip concave profile error

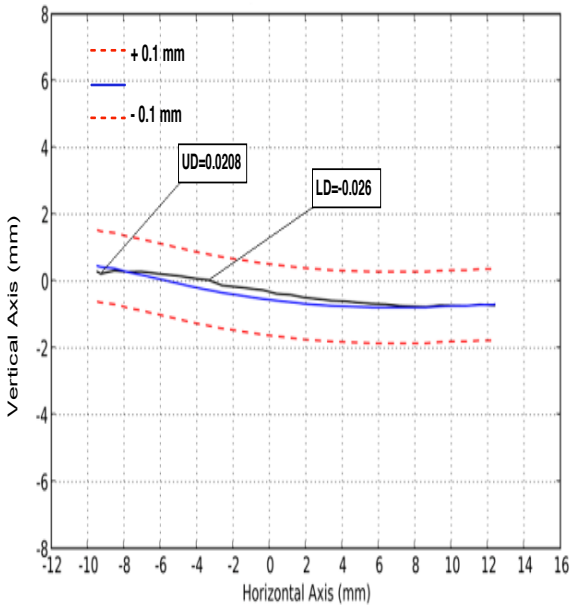

Figure 23 CMM tip concave profile error

ACCEPTED MANUSCRIPT

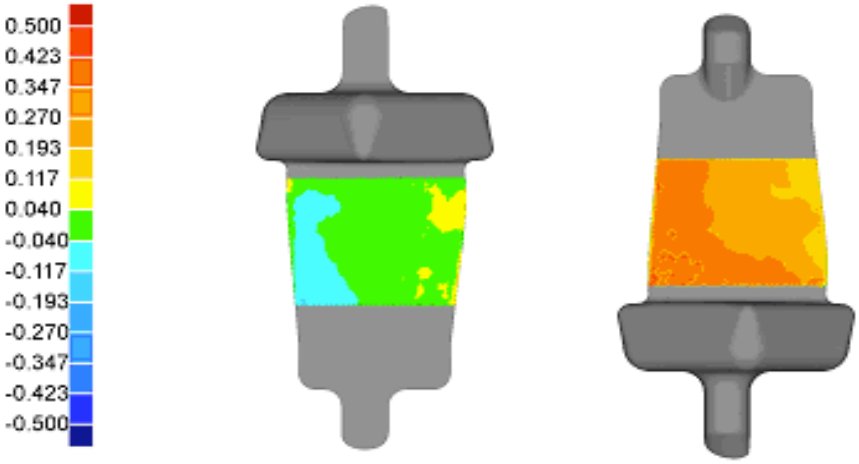

Figure 24 Deviation of (a) concave and (b) convex surface from nominal for 3-2-1 registered model

ACCEPTED MANUSCRIPT

ACCEPTED MANUSCRIPT

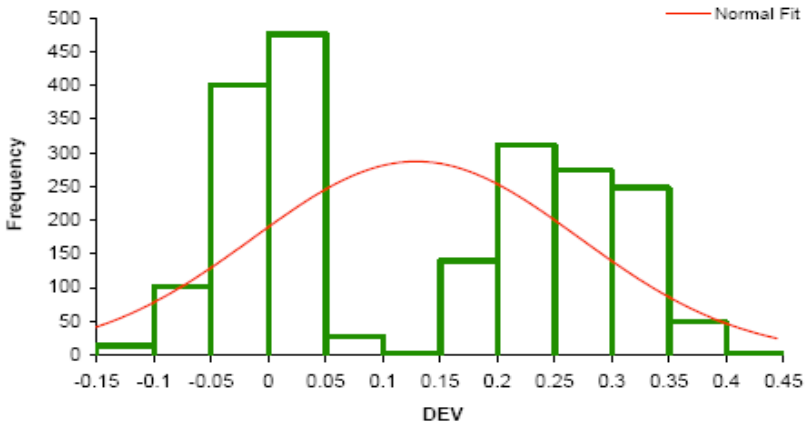

Figure 25 Histogram of frequency distribution for deviation from nominal of 3-2-1 registered model

ACCEPTED MANUSCRIPT

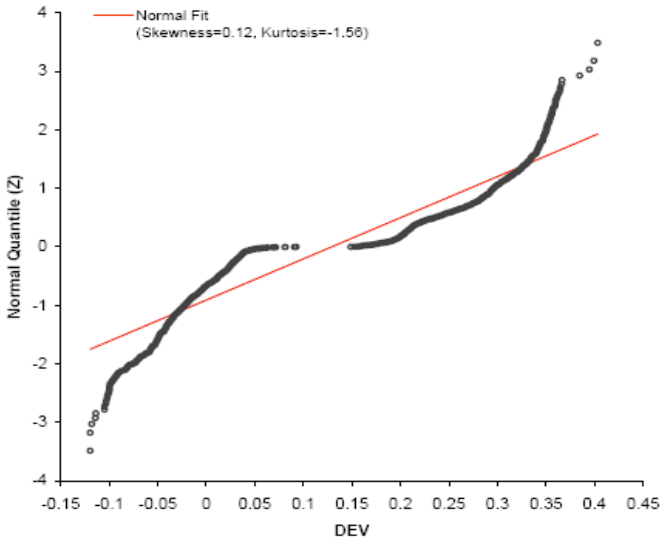

Figure 26 Normal probability plot for deviation data of 3-2-1 registered model

ACCEPTED MANUSCRIPT

ACCEPTED MANUSCRIPT

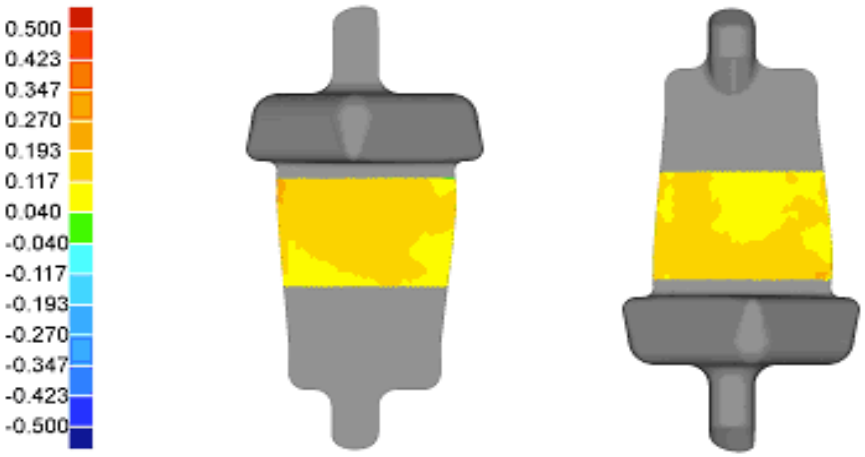

(a) (b)

Figure 27 Deviation of (a) concave and (b) convex surface from nominal for the ICP localised model

ACCEPTED MANUSCRIPT

ACCEPTED MANUSCRIPT

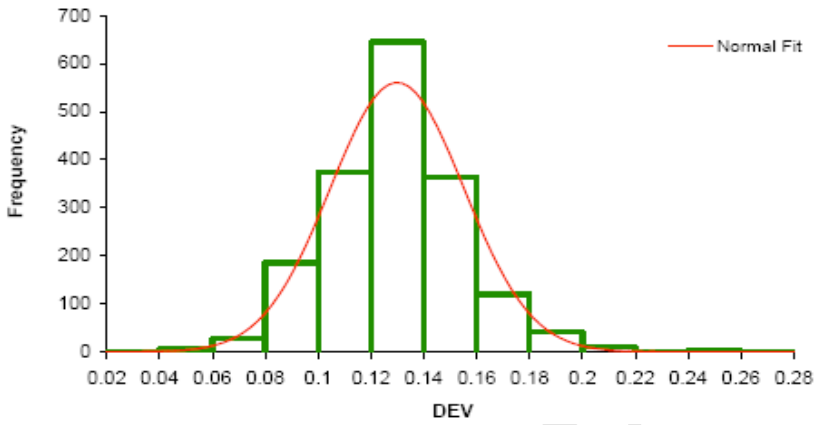

Figure 28 Histogram of frequency distribution for deviation from nominal of ICP localised model

ACCEPTED MANUSCRIPT

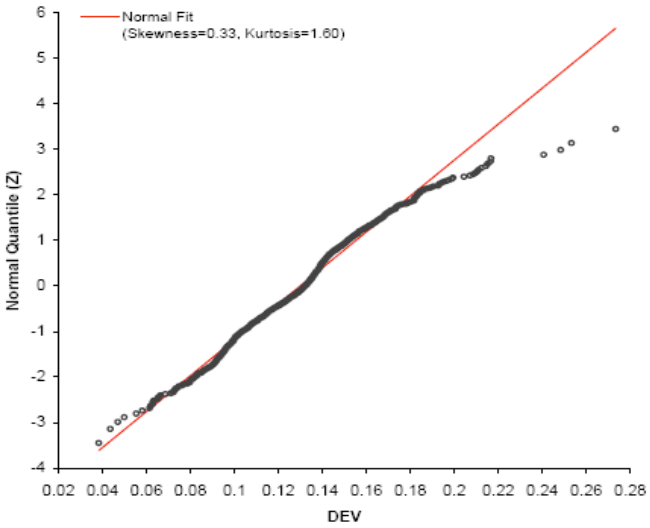

Figure 29 Normal probability plot for deviation data of ICP localised model

Table 1 Description of dimensional errors

Error	Description	Calculation
Thickness	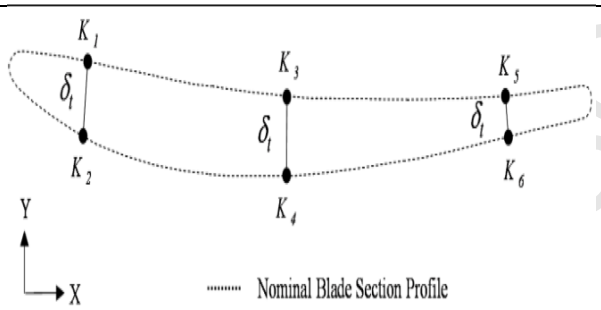	$\delta_t = \lvert K_{CC} - K_{CV} \rvert$ (1) $\delta_1 = \delta_t^{'} - \delta_t$ (2)
Twist	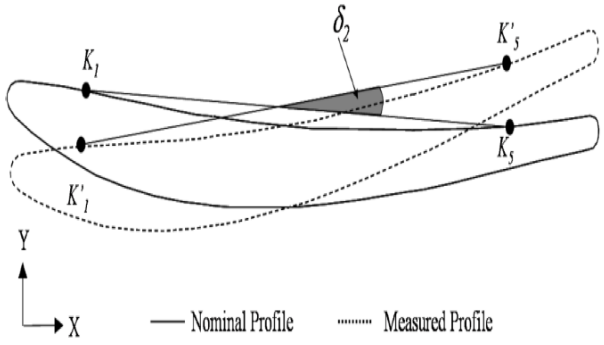	$\delta_2 = \cos^{-1}\left(\frac{\vec{K_1K_5} \bullet \vec{K'_1K'_5}}{\lvert\vec{K_1K_5}\rvert \lvert\vec{K'_1K'_5}\rvert}\right)$ (3)
Bow	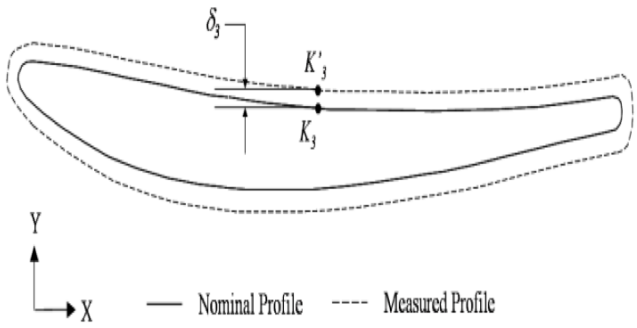	$\delta_3 = K_{3y}^{'} - K_{3y}$ (4)

Table 2 Profile error comparison

Profile Error		RMS (mm)	Stand Dev (mm)	*p* value	Significant?
Root Convex	CMM	0.016	0.013	0.122	NO
	Virtual	0.021	0.015		
Mid Convex	CMM	0.013	0.014	0.741	NO
	Virtual	0.012	0.012		
Tip Convex	CMM	0.017	0.014	0.224	NO
	Virtual	0.012	0.011		
Root Concave	CMM	0.020	0.012	0.026	YES
	Virtual	0.020	0.018		
Mid Concave	CMM	0.014	0.010	0.124	NO
	Virtual	0.014	0.012		
Tip Concave	CMM	0.022	0.013	0.061	NO
	Virtual	0.015	0.012		

ACCEPTED MANUSCRIPT

ACCEPTED MANUSCRIPT

Table 3 Profile error comparison

Data Source	Root Section Thickness (mm)			Mid Section Thickness (mm)			Tip Section Thickness (mm)			RMS (mm)	Stand Dev (mm)
	LE	MID	TE	LE	MID	TE	LE	MID	TE		
CMM	0.262	0.302	0.314	0.318	0.296	0.286	0.325	0.285	0.284	0.297	0.020
Virtual	0.320	0.304	0.304	0.326	0.290	0.301	0.311	0.286	0.285	0.303	0.016

*LE – leading edge, TE – trailing edge, MID – K Point 3.

ACCEPTED MANUSCRIPT

ACCEPTED MANUSCRIPT

Table 4 Bow error comparison

Data Source	Root Bow (mm)	Mid Bow (mm)	RMS (mm)
CMM	0.038	0.020	0.030
Virtual	0.043	0.024	0.034

ACCEPTED MANUSCRIPT

ACCEPTED MANUSCRIPT

Table 5 Twist error comparison

Data Source	Mid Twist Angle	Tip Twist Angle	RMS
CMM	0.114°	-0.136°	0.125°
Virtual	0.250°	0.414°	0.342°

ACCEPTED MANUSCRIPT

ACCEPTED MANUSCRIPT

Table 6 Deviation comparison between 3-2-1 and ICP localisation procedures

Deviation	3-2-1 Method (mm)	ICP Method (mm)
Max Dev (+)	0.401	0.268
Max Dev (-)	-0.119	0.000
Average (+/-)	0.183/-0.034	0.129/0.000
St Dev	0.140	0.021

ACCEPTED MANUSCRIPT

ACCEPTED MANUSCRIPT

A Virtual Inspection Framework for Precision Manufacturing of Aerofoil Components (JCAD_1927)

Jonathan E. Makem[1)], Hengan Ou[2)*] and Cecil G. Armstrong[1)]

[1)] School of Mechanical and Aerospace Engineering, Queen's University Belfast, Belfast, UK, BT9 5AH

[2)] Department of Mechanical, Materials and Manufacturing Engineering, University of Nottingham, Nottingham, UK, NG7 2RD

Highlights

The paper presents a virtual inspection framework to assess the accuracy of blades.

Both the 3-2-1 approach and the ICP method are developed for part registration.

The ICP method achieves a better solution than the 3-2-1 approach in registration.

A case study produces a good agreement in compared with actual measurement data.

* corresponding author: h.ou@nottingham.ac.uk

ACCEPTED MANUSCRIPT